Florida International University

FIU Digital Commons

FIU Electronic Theses and Dissertations | University Graduate School

7-1-2022

A Numerical Investigation of Tornado Production and Intensification in Tropical Cyclones

Marco Paredes
Florida International University, mpare054@fiu.edu

Follow this and additional works at: https://digitalcommons.fiu.edu/etd

 Part of the Atmospheric Sciences Commons, and the Meteorology Commons

Recommended Citation

Paredes, Marco, "A Numerical Investigation of Tornado Production and Intensification in Tropical Cyclones" (2022). *FIU Electronic Theses and Dissertations*. 5114.
https://digitalcommons.fiu.edu/etd/5114

This work is brought to you for free and open access by the University Graduate School at FIU Digital Commons. It has been accepted for inclusion in FIU Electronic Theses and Dissertations by an authorized administrator of FIU Digital Commons. For more information, please contact dcc@fiu.edu.

FLORIDA INTERNATIONAL UNIVERSITY

Miami, Florida

A NUMERICAL INVESTIGATION OF TORNADO PRODUCTION AND INTENSIFICATION IN TROPICAL CYCLONES

A thesis submitted in partial fulfillment of

the requirements for the degree of

MASTER OF SCIENCE

in

GEOSCIENCES

by

Marco Paredes

2022

To: Dean Michael Heithaus
College of Art, Sciences, and Education

This thesis, written by Marco Paredes, and entitled A Numerical Investigation of Tornado Production and Intensification in Tropical Cyclones, having been approved in respect to style and intellectual content, is referred to you for judgment.

We have read this thesis and recommend that it be approved.

_____
Hugh Willoughby

_____
Haiyan Jiang

_____
Ping Zhu, Major Professor

Date of Defense: July 1, 2022

The thesis of Marco Paredes is approved.

_____
Dean Michael Heithaus
College of Art, Science, and Education

_____
Andrés G. Gil
Vice President for Research and Economic Development
and Dean of the University Graduate School

Florida International University, 2022

© Copyright 2022 by Marco Paredes

All rights reserved.

DEDICATION

I dedicate this master's thesis to my late mother Maria Elena Trozz. You were there for me every step of the way, even when all seemed lost. While you could not see the final product, I could not reach the end without you. I also dedicate this thesis to my father Angel Javier Trozz and my brothers Victor and Eduardo Paredes. Constant love and encouragement have brought me to where I am now. I could not have had a better family.

ACKNOWLEDGMENTS

I would like to acknowledge my major professor Ping Zhu for taking a chance on me and helping throughout my master's program. I am mostly thankful for allowing me to pursue a project that really stokes my interest. Your constant care and availability to help me with even the smallest problems has made my master's career not only educational but enjoyable. I would also like to thank my academic committee whose support and knowledge has opened many paths to take in research and stoked my love in meteorology. Finally, I would like to thank the FIU meteorology cohort. Through my undergraduate and graduate career, we all have been through thick and thin and in the end the sense of community and support made the journey more enjoyable. This thesis is supported by NOAA/HFIP under Grants NA16NWS4680029 and NA18NWS4680057 and National Science Foundation (NSF) under Grant AGS-1822238.

ABSTRACT OF THE THESIS

A NUMERICAL INVESTIGATION OF TORNADO PRODUCTION AND INTENSIFICATION IN TROPICAL CYCLONES

by

Marco Paredes

Florida International University, 2022

Miami, Florida

Professor Ping Zhu, Major Professor

The environmental conditions required for tornado formation and development in tropical cyclones (TCs) and the mechanisms underlying the intensification of TC tornadoes remain poorly understood. Previous research has suggested that low and mid-level dry air intrusion in TCs may enhance convective instability and influence the production of tornadoes. However, observations have their limitations in answering some of the key questions regarding the relationship among thermodynamic instability, dry air, and TC tornado genesis, development, and dissipation. In this study, a multiple nested Weather Research and Forecasting (WRF) model in a hindcasting mode is used to simulate Hurricane Ivan (2004) by resolving tornadoes, the supercells that spawn tornadoes, TC vortex, and large-scale environmental flow in a unified system. The characteristics of vorticity generation, updraft and downdraft couplets of supercells, and convective environments are extracted and investigated. By obtaining quantitative data relevant to TC tornados, this study tackles some of the long-standing questions concerning TC tornado-genesis and rapid intensification of TC tornadoes.

TABLE OF CONTENTS

LIST OF FIGURES

ABBREVIATIONS AND ACRONYMS

ARW	Advanced Research WRF
CAPE	Convective Available Potential Energy
CIN	Convective Inhibition
LES	Large Eddy Simulation
NCAR	National Center for Atmospheric Research
NCEP	National Center for Environmental Prediction
NCEP FNL	NCEP Final
NCL	NCAR Command Language
NHC	National Hurricane Center
QNSE	Quasi-Normal Scheme Elimination
RH	Relative Humidity
RRTM	Rapid Radiative Transfer Model
SGS	Sub-grid Scale
SPC	Storm Prediction Center
SRH	Storm Relative Helicity
TC	Tropical Cyclone
TCTOR	Tropical Cyclone Tornado
TKE	Turbulent Kinetic Energy
TSK	Temperature of the Surface Skin
VWS	Vertical Wind Shear
WRF	Weather Research and Forecasting model

CHAPTER 1. INTRODUCTION

Landfalling tropical cyclones (TCs) have produced tornadoes from coastal communities to locations hundreds of miles inland. TC tornadoes pose a difficult challenge for forecasters to warn owing to their weaker and shallower nature than their mid-latitude counterparts, causing traditional radar signatures such as hook echoes and velocity couplets to become obscured by the parent circulation (Spratt 1997, McCaul et al. 2004). It is essential to document and understand the thermodynamic and kinematic environments that spawn these tornadoes in landfalling TCs. Doing so will allow a more comprehensive understanding of the dynamic response of tornadoes in each storm environment, allowing for a more accurate forecast of their behavior.

TC tornadoes often form in the late afternoon in the outer region of a TC (~100-500 km from the TC center) approximately 48 hours before and after TC landfall (Novlan 1974, Edwards 2012). These tornadoes often form in the northeast quadrant of TCs, where the veering profile of the wind is more conducive for tornadogenesis than the other quadrants (Novlan and Gray 1974, McCaul 1991, Edwards 2012). Compared to their midlatitude counterparts, TC tornadoes are generally weaker and briefer (Edwards 2010, Edwards 2012) and form in "miniature supercells," which are shallower, weaker, and shorter-lived than the midlatitude supercells (McCaul 1991, McCaul Weisman 1996, Spratt 1997, Baker et al. 2009). Eastin and Link (2009) found that the average mesocyclone diameter in TC tornadoes is 6 km and has an average depth of 4 km, compared to the Great Plains supercells, which have an average mesoscale diameter of 10 km, and a depth of 9 km. Figure 1 shows a sketch that conceptually demonstrates the

differences between these two types of supercells that spawn mid-latitude and TC tornadoes respectively (adopted from Eastin 2004). While smaller, TC "miniature supercells" contain strong vertical wind shear (VWS) and favorable thermodynamic instability in the low troposphere sufficient for producing tornadoes.

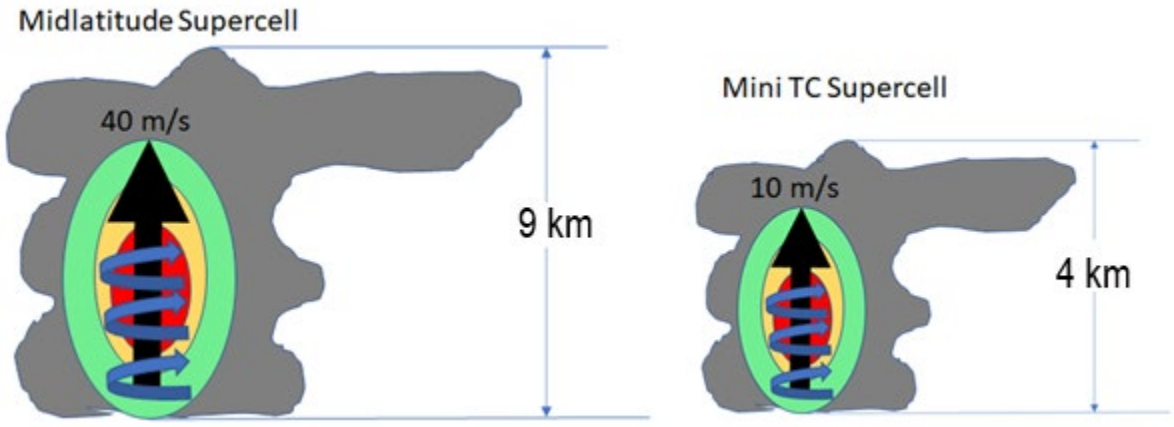

Fig. 1: Schematic illustration of mid-latitude supercell and miniature TC supercell (after Eastin 2004).

Despite being weaker and shallower, TC tornadoes differ from non-TC tornadoes not so much in their process or ingredients of production but rather in the ingredients' magnitude and spatial position. One requirement for tornadogenesis is VWS. VWS determines the amount of horizontal vorticity that will ultimately be tilted into the vertical and provide the tornado rotation. In TCs, VWS is mostly contained to the bottommost layer of the troposphere, the so-called boundary layer, and is larger than that of midlatitude supercells (McCaul 1991, Schenkel 2020). Gentry (1983) stated that TC tornadoes often form in areas where the 850 mb winds are enhanced. As the TC rainband moves ashore, the frictional forces of the land mass will slow down the low-level winds while the winds 1-3 km above the ground remain unaffected, causing a greater increase in

the low level VWS. VWS also alters the TC convective structure and, consequently, alters the location of TC tornadoes. A normal TC with no VWS may be considered as an axisymmetric low-pressure system with a primary horizontal circulation superimposed with a secondary overturning circulation induced by the friction and TC eyewall convection. VWS causes the TC vortex to become increasingly tilted with height, which can weaken the TC vortex. To compensate, TCs will enhance the secondary overturning circulation in the downshear half to restore the gradient wind balance at the vortex scale. Conversely, descent and retardation of the TC's secondary circulation dominates the upshear quadrants of a TC. Both forces act together to cause the precipitation, and by proxy, tornadoes to be increasingly isolated to the downshear half of a TC (Schenkel 2020). Figure 2 depicts a plane view of tornado locations relative to westerly shear (panels a, c, and e) and relative to true north (b, d, and f) respectively for TCs in strong, medium, and weak shear (Schenkel 2020). The increasing VWS causes the tornado location to become entirely localized to the downshear quadrants. The radial relationship does not appear to change with increasing shear. Typically, the tornadoes closest to the TC center (~ 100 km) are in the downshear left quadrant, whereas the tornadoes furthest from the TC center (~350 km) are in the downshear right quadrant. Understanding VWS in the outer rainband environment is paramount to a better understanding of the behavior of TC tornadoes.

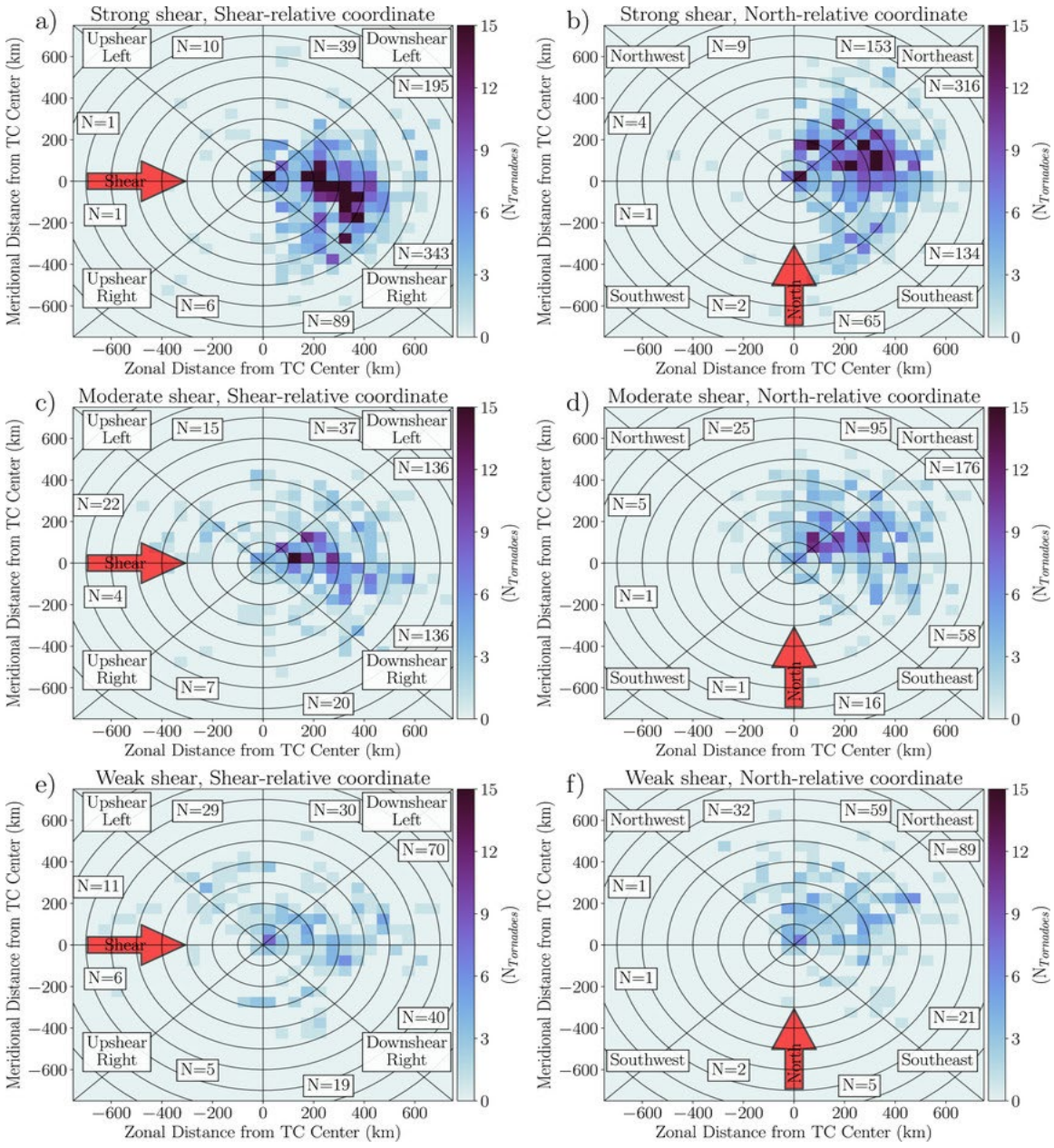

Fig. 2: Plane view plots of tornado locations ($N_{tornadoes}$; shaded squares) for TCs in (a),(b) strong; (c),(d) moderate; and (e),(f) weak VWS. Tornado reports in (a), (c), and (e) have been rotated around the TC center such that the VWS vector (red arrow) at the time of tornado occurrence is pointing to the right. The tornado reports in (b), (d), and (f) are plotted relative to true north with the red arrow labeled accordingly. The boxed numbers show the total number of tornadoes in each octant. (After Schenkel 2020)

Thermodynamic instability is generally considered necessary for tornadogenesis. However, the role of instability in TC tornadogenesis and intensification remains controversial. Thermodynamic instability is often measured by the convective available potential energy (CAPE), defined as a cumulative (or vertically integrated) difference in temperature between a rising adiabatic air parcel and its environment. Early works on investigating the thermodynamic requirements of TC tornadoes have found that the CAPE values of the environment in which TC tornadoes are embedded are much lower than those of the mid-latitude systems. McCaul (1991) analyzed hundreds of rawinsondes in proximity to TC tornadoes and found that the average CAPE values vary from 300 J/kg to 1200 J/kg, with the highest CAPE in the right quadrant relative to TC motion towards the outer radii. These values are nowhere close to the CAPE values in the mid-latitude (>2500 J/kg) that spawn tornadoes. This reduced CAPE is primary reason for supercells in TC environments to be shallower than their midlatitude counterparts (McCaul & Weisman 1996). Moreover, McCaul (1991) noted that there is a somewhat weak negative correlation between the CAPE values and tornado outbreak severity that is statistically significant at the 23% level. This result seems to be supported by other studies (e.g., Viseco 1996; Molinari 2010; and Sueki 2016) that have found that CAPE is an unimportant factor in determining the severity of TC tornado outbreaks, particularly concerning other factors such as helicity and VWS. Onderlinde (2014) studied 28 potential predictors for TC tornados, including CAPE, shear, distance from the TC center, etc., and developed a statistical guidance product for forecasting TC tornadoes in the north Atlantic basin. Surface-based CAPE only has a small correlation coefficient of 0.16

compared to a correlation coefficient of 0.48 between 0-6km VWS and tornado production.

In contrast, some other studies show that CAPE may play a role in determining TC tornado genesis and severity. For example, Baker (2009) conducted a similar rawinsonde analysis to McCaul (1991) for mini supercells in Hurricane Ivan's rainband. His results show that while the cells spawning tornadoes had average amounts of shear and helicity, they do have higher than average CAPE values. The relevance of CAPE to tornadogenesis becomes especially clear when Hurricane Jeanne made landfall in the same year with the same intensity, shear distribution, and helicity distribution as those of Ivan but did not produce tornadoes. One apparent disparity between the two storms is that Ivan had much higher CAPE values than Jeanne, as seen in Figure 3**,** suggesting that the elevated CAPE may play a critical role in Ivan's high tornadic activities during its landfall. As pointed out by McCaul (1991), the negative correlation between CAPE and tornado severity seen from the data analyses should not be used as a base to deemphasize the importance of instability to TC tornado production; rather, it suggests that how instability in conjunction with dynamical factors leads to TC tornado outbreak remains poorly understood. Even if the CAPE is on the order of a few hundred, if sufficient buoyancy is located near the surface, then the induced updraft in the presence of favorable shear may potentially create a tornado.

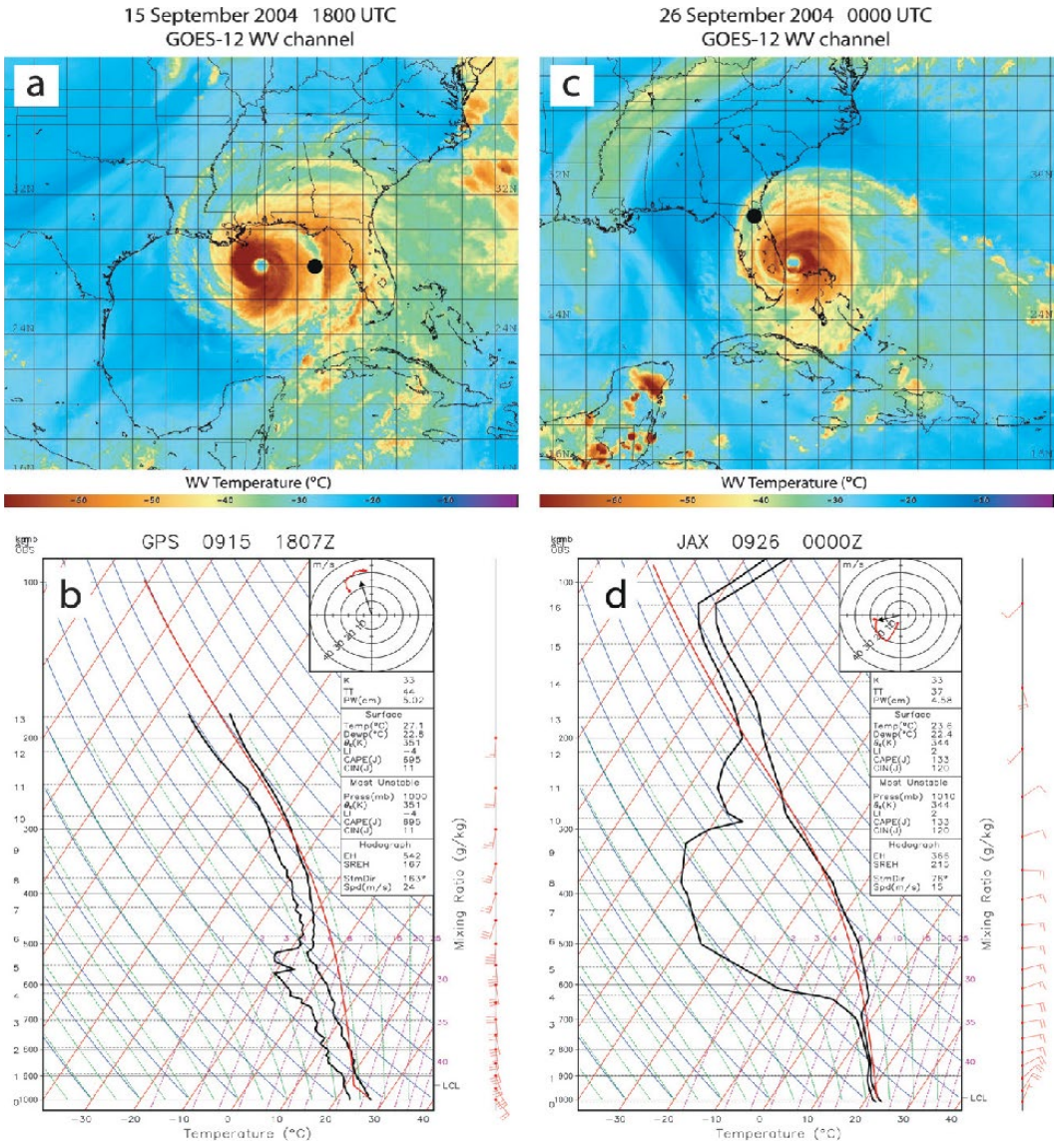

Fig. 3: GOES water vapor imagery for (a) Hurricane Ivan at 1815 UTC Sep 15 2004 and (c) Hurricane Jeanne at 0015 UTC Sep 26 2004. Skew-T diagrams for (b) global positioning system (GPS) dropsonde deployed in 1807 UTC Sep 15 and (d) KJAX rawinsonde launched 0000 UTC Sep 26 within Ivan and Jeanne respectively. Black circles in (a) and (c) are the location of the respective sounding. (after Baker 2009).

The third factor that can influence the production of TC tornadoes is mid-level dry air intrusion (e.g., Hill et al. 1966, Novlan and Gray 1974, McCaul 1987, Curtis 2004, Feliciano 2016). McCaul (1991) noted that dryness in the mid-level of the

atmosphere could alter the thermodynamic structure of supercells by enhancing surface-based CAPE and instability, but the relationship between the mid-level dryness and the enhanced CAPE was not apparent in his dataset. Curtis (2004) conducted a study that collocated TC tornado clusters with mid-level tropospheric drying using the data collected from 1960-1999 and found that of the 13 'outbreaks' that produced 20 or more tornadoes, 11 had apparent dry intrusions in the mid-level before the outbreaks. He further showed that the outbreaks occurred when there was a pronounced relative humidity (RH) gradient in the layer of 700 -500 hpa in the right front (or northeast) quadrant of TCs. Feliciano-Camacho (2016) expanded this study to all TCs in the Atlantic basin regardless of intensity that made landfall in the United States and produced 6+ tornadoes in 24 hours using the European Centre for Medium-Range Weather Forecasts ERA-Interim reanalysis data in the years of 2000 – 2014. By categorizing the percentage of tornadoes based on the RH gradients at 300, 400, 500, and 700 hPa, Feliciano-Camacho (2016) found that 42 of 62 (68%) individual outbreaks were collocated with the large RH gradients at 500 hPa. Moreover, the analyses revealed that the location and orientation of the dry slot are often offset from the tornado outbreak locations with most tornado outbreaks having dry air ahead or behind the systems. Several mechanisms have been proposed to explain the observed relationship between TC tornado outbreak and mid-level dry air intrusion. These include enhancing atmospheric instability by dry air (Hill 1996); creating low-level baroclinicity at the boundaries between clear and cloudy air (McCaul 1987, Curtis 2004), which can assist vertical tilting of horizontal vorticities; and promoting evaporative cooling through entraining dry air into the storm (Edwards 2010). The resultant downdrafts can trigger

further development of updrafts resulting in more severe storms. However, the exact route to TC tornadogeneisis via mid-level dry air intrusion remains unclear.

In addition to VWS, helicity, CAPE, and mid-level dry air intrusion, some degree of convective inhibition associated with the capping inversion at the top of the boundary layer is commonly believed to be critical to the formation of mid-latitude tornadoes since the inversion acts as a cap to trap moisture and heat within the boundary layer. As the boundary layer gets warmer and more humid, the cap becomes weaker. Once the cap is broken, explosive thunderstorms can develop, which may spawn tornadoes. However, this mechanism, may not play a critical role in TC tornadogenesis since CAPE in TCs is not mainly generated through surface heating and moistening and the capping inversion usually does not exist or is very weak within the outer rainband regions where tornadoes generally form.

Helicity is a measure of an updraft's potential for helical flow and is often used to estimate the probability of supercell development. Computed form the 0-3 km vertical wind profile, relative to storm motion, helicity is proportional to updraft strength, vorticity, and vertical wind shear. Helicity in TC supercells are lower than average values found in midlatitudes however, TC supercells demonstrate an asymmetric distribution of helicity, with higher helicity found in the favorable downshear quadrant.

While the unprecedented datasets collected by dropsondes and Doppler radars have provided valuable first-hand knowledge of precursors and conditions for TC tornadogenesis and tornado characteristics, many questions regarding the initiation and intensification of tornadic vorticities cannot be solely answered by observational data. The limitations of both spatial and temporal resolution of observations are often too low

to provide key four-dimensional dynamic and thermodynamic information at the tornado scales. Locating rotational features is still quite difficult especially at further distances from the radar. Velocity couplets in TC tornadoes can appear and disappear between scans and features such as hook echoes and appendages may become too subtle for a clear identification (Schneider 2007).

With the advances in computational technology and ever-increasing computational power, numerical simulations of tornadoes have emerged as an attractive powerful tool to tackle the unanswered issues of tornadoes. Tornado-resolving simulations to date have been mostly performed in idealized settings in which tornado precursor is often prescribed in the initial field. Simulations are driven by horizontally homogeneous large-scale forcing and supplied with periodic lateral boundary conditions. Early attempts used small domain but high enough resolution to resolve artificially forced tornado vortex (e.g., Fiedler 1994; Lewellen et al. 2000). Because of the small model domain, the tornado parent storm (or supercell) was not included in these simulations. Later with larger model domains, both tornadoes and the supercell in which tornadoes are embedded can be simulated simultaneously (e.g., Xue 2004; Roberts et al. 2016; Orf et al. 2017). Although more realistic since the tornadoes in the simulations are not artificially forced but are generated from the parent supercells, these simulations are still idealized in that the prescribed ambient conditions of supercells are assumed to be horizontally homogeneous otherwise the periodic lateral boundary conditions cannot be applied. The idealized simulations may be appropriate for investigating mid-latitude tornadoes and their parent supercells, but such a numerical method becomes questionable when it is applied to simulating TC tornadoes since a TC vortex is a moving target, and

the swirling TC winds change their direction and speed continuously, which causes the assumption of horizontally homogeneous environment to be invalid. For this reason, in this study I use a different approach to simulate TC tornadoes, their parent supercells, and TC vortex in a unified system in a hindcasting mode. The detailed numerical method used for this study will be described in Chapter 2. Using the real-case simulation of Hurricane Ivan (2004), I aim to fulfill the following three research objectives,

1. Performing hind-casting real-case WRF simulations of Hurricane Ivan to see if tornadoes can be generated spontaneously by the convective cells in the outer rainbands at the location of observed tornadoes without an artificially prescribed tornado precursor.

2. Examining the environmental conditions including VWS, CAPE, and RH in which TC tornadoes are embedded and testing the hypothesis that elevated CAPE and mid-level dry air intrusion are critical to TC tornadogenesis and tornado outbreak.

3. Exploring the source of TC tornado vorticity and the causes of tornado intensification.

CHAPTER 2. NUMERICAL METHODOLOGY

a. LES BACKGROUND

Numerical simulations of tornadoes require model grid resolution to be high enough to resolve large energy-containing turbulent eddies. This type of simulation is known as large-eddy simulations (LESs). One requirement for LESs is that mode grid spacing must fall in the Kolmogorov inertial subrange (Kolmogorov 1941) on the turbulence energy spectrum so that only small-scale turbulence needs to be parameterized. Since turbulence with scales smaller than inertial subrange contains much less energy and is less flow-dependent than large energy-containing eddies, the LES methodology is commonly thought to be insensitive to formulaic details and arbitrary parameters used in the turbulent mixing parameterization. Thus, the turbulent flow generated by LESs are often used as a proxy for reality and a basis for understanding turbulent flow and guiding theories when direct observations are difficult to obtain. Classic LESs, including those used for simulating tornadoes, use an idealized setting in which simulations are initialized and forced by horizontally homogeneous large-scale forcing. As stated previously, this idealized setting is not appropriate to simulate TC tornadoes because of the non-stationary and heterogeneous nature of TC vortex flow. To solve this problem, Zhu (2008a; 2008b; and Zhu et al. 2015) used a different approach to simulate the TC boundary layer flow by gradually scaling a real-case convection permitting regional simulation down to an LES domain utilizing the two-way interactive nesting technique. The nested LES in a hindcasting mode allows the large turbulent eddies, including the roll vortices generated by the convective instability and inflection-

point instability in the TC boundary layer, to be explicitly simulated in a realistic TC environment.

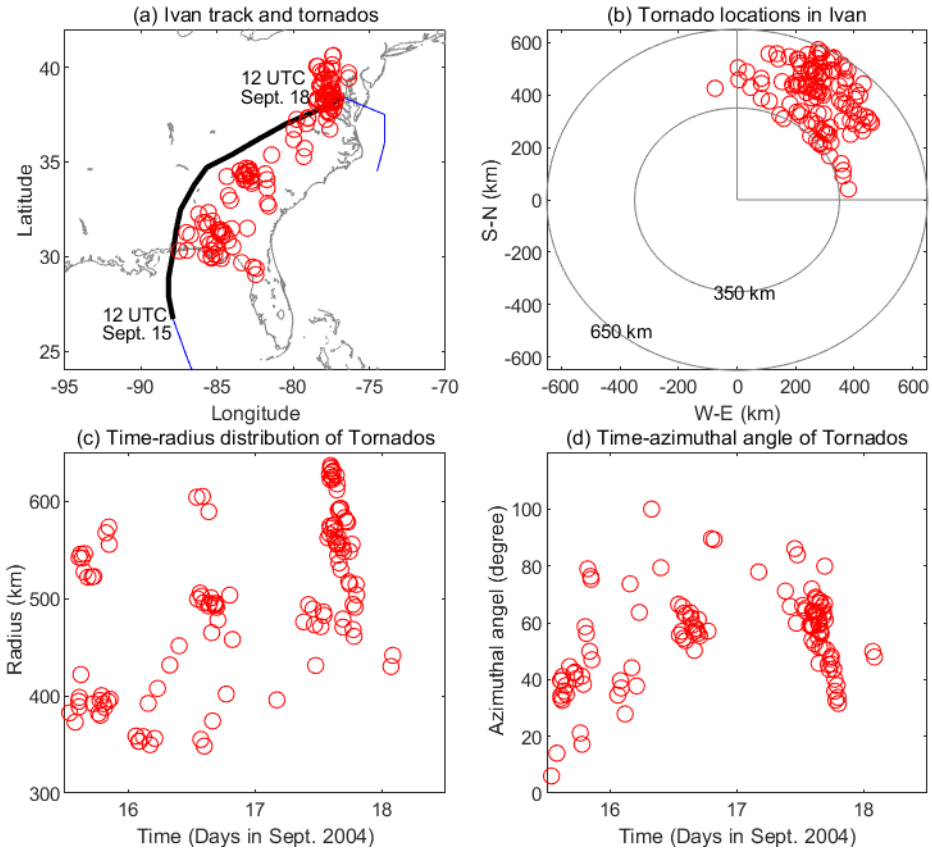

Fig. 4: (a): Geographic locations of recorded tornadoes and the best-track of Ivan (2004); (b): Tornado locations in a cylindrical coordinate centered at the storm center; (c) and (d): Tornado distribution as the function of time, radius, and azimuthal angle, respectively.

b. OBSERVED TORNADOES IN HURRICANE IVAN (2004)

This study uses the multiple two-way nested simulation framework to simulate TC tornadoes formed in Hurricane Ivan (2004). Ivan (2004) is on record for having the most tornadoes produced in its lifetime at 118 tornadoes during its three-day journey through the United States. Ivan (2004) produced TC tornadoes at nearly every configuration, from forming waterspouts offshore before making landfall to creating new cells entirely overland, spawning tornadoes when the storm transitioned from TC to an extratropical cyclone. Figure 4 shows the locations, occurring time, radial distances from the storm center, and azimuthal angles from north of all recorded tornados generated by Ivan (2004). All tornadoes in the three-day period during the landfall from 12 UTC Sept. 15 to 12 UTC Sept. 18 occurred in the outer rainband region with the radii from 350 km to 650 km and in the right-front quadrant with respect to the storm track. The abundant tornadoes spawned in the outer rainband regions of Ivan makes the storm ideal for numerical investigation of TC tornadoes.

c. MODEL CONFIGURATION

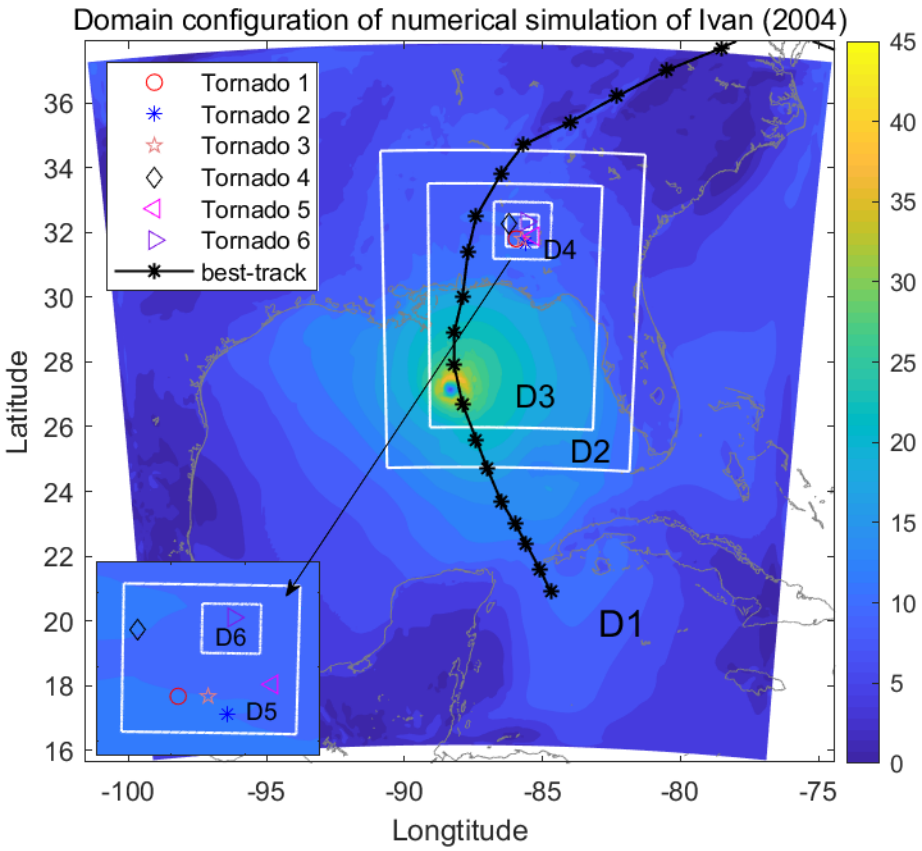

Fig. 5: Domain configuration of WRF simulation of Hurricane Ivan (2004). It consists of 6 domains. The background shades are the 10-m wind speed at 15 UTC Sept. 15, 2004. Symbols ∘, ∗,, ◊, ◁, and ▷ indicate the observed tornadoes.

To appropriately simulate both the evolution of Ivan and the tornadoes spawned by Ivan, I conducted a multiple nested simulation of Ivan using the Weather Research and Forecasting (WRF) model with the Advanced-Research WRF (ARW) dynamic core (Skamarock et al., 2008). It consists of 6 domains: one parent domain and 5 two-way nested subdomains, as illustrated in figure 5. Domain D1, with a grid resolution of 8100 m, covers the entire Gulf of Mexico, part of the Atlantic and Caribbean, and most of the

US so that the large-scale flow pattern can be realistically simulated. To obtain a better hurricane vortex structure, domains D2 and D3 with horizontal resolutions of 2700 m and 900 m respectively are configured large enough to cover the entire hurricane vortex during the landfalling period from 12 UTC Sept. 12 to 12 UTC Sept. 18 when most of the tornadoes occurred. The high-resolution domains, D4, D5, and D6 with grid resolutions of 300 m, 100 m, and 33.33 m respectively, are chosen at the locations where tornadoes occurred during 15 UTC – 18 UTC Sept. 15, according to the observations. Six of the observed tornadoes in domain D6 are marked in figure 5. A total of 74 levels are configured in the vertical for all domains. 19 and 12 layers are below 2 km and 1 km, respectively. In short, the domain configuration shown in figure 5 is designed to obtain the best simulation of the hurricane vortex so that the tornadoes can be generated in an environment as realistic as possible with our available computational power.

A key model physics in this multiple-scale WRF simulation of TC tornadoes is how to treat the sub-grid-scale (SGS) turbulent mixing. At the LES resolution, only small-scale isentropic turbulence needs to be parameterized. Following the LES methodology, both horizontal and vertical SGS mixing of domains D4, D5, and D6 is parameterized by the three-dimensional turbulent kinetic energy (TKE) scheme (Deardorff, 1980), which is built within the model dynamic core. Large energy-containing eddies are not resolved for domains D1, D2, and D3. These large anisotropic eddies cause the vertical turbulent mixing to be significantly different from horizontal turbulent mixing, and thus, they must be treated differently. A common method is to have a standalone vertical turbulent mixing scheme outside the model dynamic core to overwrite the built-in three-dimensional SGS mixing scheme. In this study, the one-

dimensional Quasi-normal scale elimination (QNSE) scheme (Sukoriansky et al. 2005) is activated to parameterize the vertical turbulent mixing in domains D1, D2, and D3. Other major model physics include the Rapid Radiative Transfer Model (RRTM; Mlawer et al., 1997) for longwave radiation, the Dudhia scheme for short-wave radiation (Dudhia, 1989), the Morrison 2-moment scheme for microphysics (Morrison et al., 2009), the unified Noah land surface model for land surface processes (Tewari et al. 2004), and the Kain–Fritsch cumulus scheme for deep convection (Kain and Fritsch, 1993) in D1 (the cumulus scheme is not activated in D2 – D6).

The 6-hourly NCEP FNL (Final) Operational Global Analysis data with 1 degree resolution is used for supplying the initial and boundary conditions of the simulation and a bogus vortex with the same size and intensity as reported in the NHC best-track is inserted in the initial fields. The simulation in domains D1, D2, D3, D4, and D5 starts at 12 UTC Sept. 15 and ends 00 UTC Sept. 17, 2004. Restart files are saved every 20 min. The outputs in D5 are used to examine if tornado-like vortices are formed. Once a well-defined tornado-like vortex is identified, I rerun the simulation with domain D6 activated using the restart file saved at the time before the identified tornado-like vortex forms. The new simulation ends after the simulated tornado dissipates. Model output in D6 is saved every 5 seconds so that the detailed time evolution of the tornado is recorded.

To investigate the effects of convective instability and mid-level moisture on the formation and structure of the TC tornado, two additional model runs were conducted using the restart file from the baseline simulation saved at the time before the tornado forms. Each new model run features only one singular modification to the environmental parameters. These modifications were made to the restart files using NCAR Command

Language (NCL). In the second model run, the surface skin temperature in domain D6 is raised by 2 degrees Celsius. This method increases air parcels' temperature near the surface, creating higher CAPE values while not affecting the environmental temperature lapse rates. This simulation allows us to examine the changes of the tornado to the artificially increased CAPE. The third model run investigates the impact of moisture in-between 300 – 700 hPa on the simulated TC tornado. These levels were chosen in light of Curtis (2004) and Feliciano (2016) who identified the dry air intrusion in these layers as the most critical to tornado outbreaks in TCs. We artificially increased RH to 80% for anywhere in-between 300 -700 hPa whose RH is below 80%. This increase of RH mitigates the presence of mid-level dry air. Differences between the three model runs will allow us to investigate the potential impact of increased instability and reduced mid-level dry air on TC tornado outbreak potential.

CHAPTER 3 BASELINE RESULTS

a. BASELINE ENVIRONMENTAL FIELD

The multi-scale WRF simulation successfully reproduced an outer convective rainband in the front right quadrant of Hurricane Ivan. Figure 6a shows a section of the rainband captured by domain D2 at 22:10 UTC several minutes after initialization. The mini-cyclone is located approximately 400 km away from the TC center and forms entirely on land. Figure 6b uses model simulation results from domain D4 to zoom in on the rainband of interest. The rainband consists of several isolated convective storms that agree with previous radar observations (Baker 2009). Some of the convective storms have characteristics similar to midlatitude supercells, including a hook-shaped distribution of hydrometeors. This weak-echo bounded echo region was collocated with a mesocyclone center that featured 4 hPa pressure fall (Figure 6c). Strom relative winds circulate cyclonically around the mini-cyclone center in a similar fashion to midlatitude supercells.

Figure 7 features thermodynamic profiles and hodographs of the simulated rainband at 22:13 UTC centered near the mini-cyclone. These soundings were derived by passing the temperature and wind profile of domain D6 through METpy. The rainband environment featured surface-based CAPE of 2062.1 J/kg and surface-based CIN of -26.4 J/kg, above average for inland TC tornadoes but closely matched the environmental soundings found in Hurricane Ivan (Baker 2009). Thus, the environment was thermodynamically primed for organized convection. The moisture profile sounding features a moist near surface layer and a dry air layer starting at 700 hpa. The minimum

of relative humidity was 40% located at 650 hpa, suggesting that the TC rainband was under the influence of the nearby dry air intrusion. The TC environment showed great kinematic potential for supercell development with 0-1 km SRH values of 87.2 m^2 /s^2 and veering of winds with height. This environment is most favorable for supercell development.

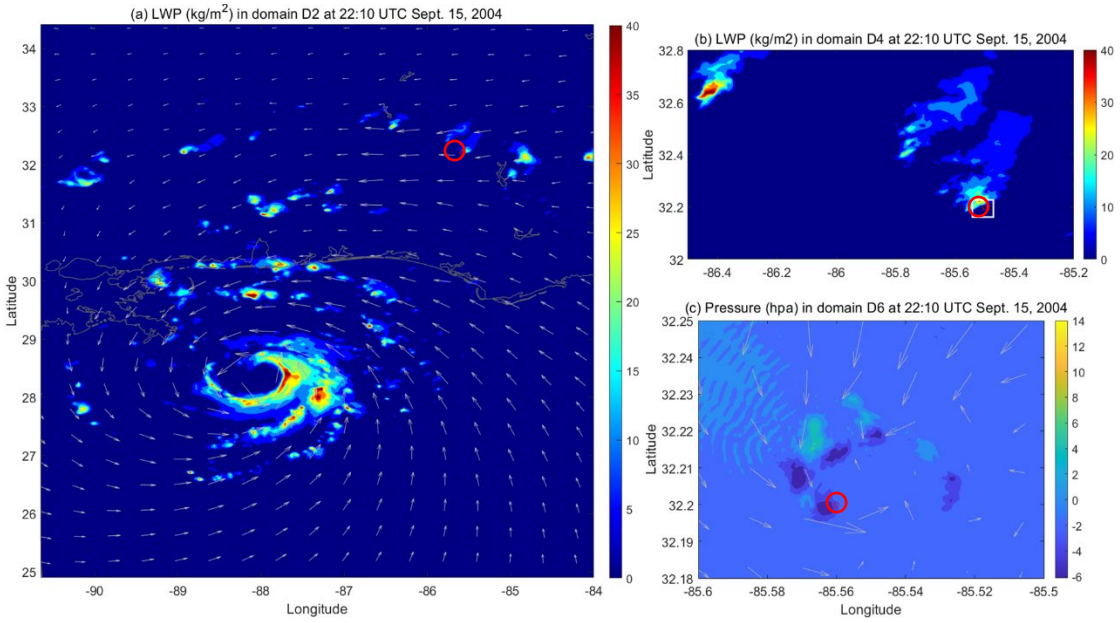

Fig. 6: (a) Liquid water path (LWP, kg/m^2) and surface winds of Ivan (2004) simulated by domain D2 at 22:10 UTC on Sept. 15, 2004. Red circle indicates the location where a TC tornado forms. (b) LWP in domain D4. (c): Pressure perturbation in domain d6 white arrows indicate direction of storm relative surface winds

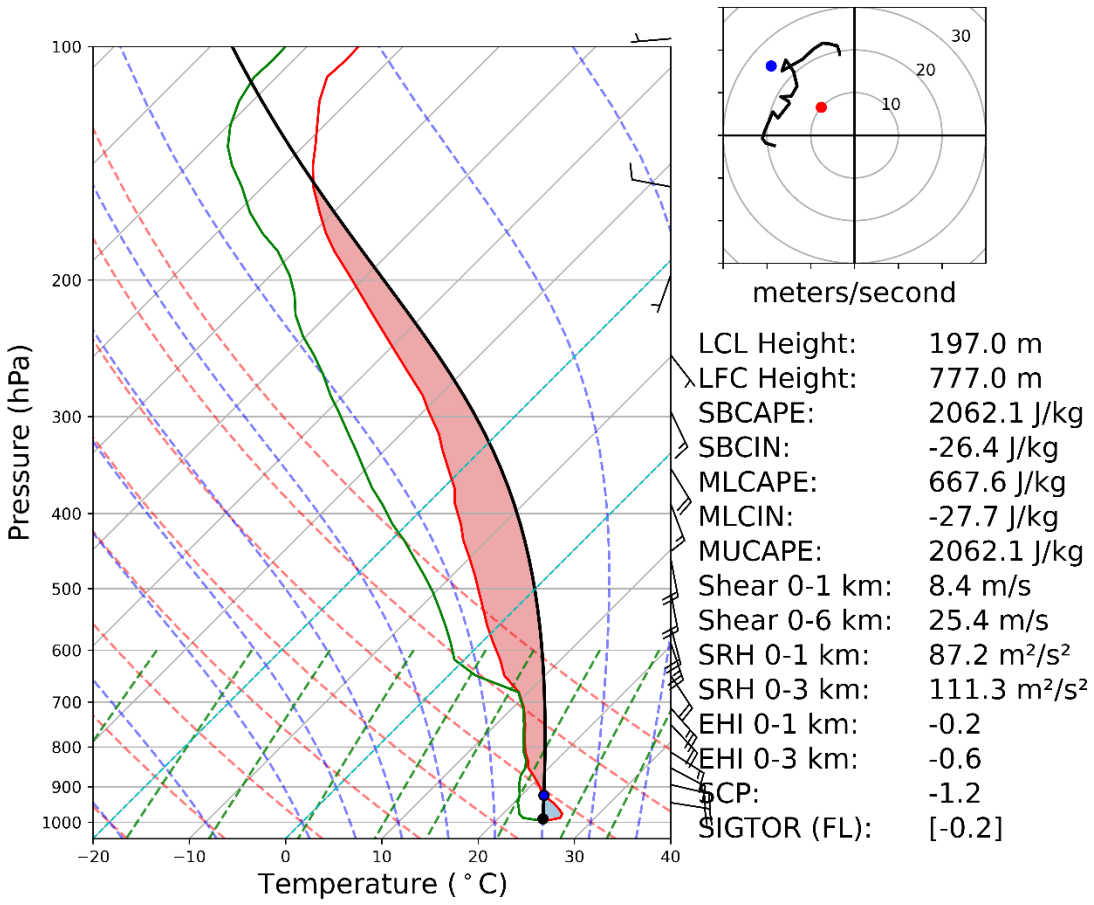

Fig. 7: Simulated SkewT-logp and hodograph analysis sounding of Hurricane Ivan at 22:13 UTC Sept. 15, 2004. The red line is temperature, the green line is dew point, and red shading is the lowest 100-mb mixed layer CAPE. Hodograph depicts the shear magnitude from 0–6-kilometer heights. Red (blue) dots represent the Bunker's right (left) storm relative motion

b. BASELINE TORNADO STRUCTURE

This section will examine the evolution of the tornado structure using domain D6. It is important to note that the aim of this experiment was not to make a perfect duplicate of the TC tornado found in Hurricane Ivan. Rather the simulation reproduces a representative mini-supercell and associated tornado using the storm environment of Hurricane Ivan.

The tornado's life cycle may be inferred from figure 8, a time-height evolution of the mean vertical vorticity ($\frac{\partial v}{\partial x} - \frac{\partial u}{\partial y}$) and vertical velocity averaged over an area of 333x333 m^2 centered at the mini-cyclone center. The low-level mini-cyclone center is defined at the location of the maximum vertical vorticity at the height of 330 m. By 22:10 UTC enhanced cyclonic vertical vorticity of more than 0.03 s^{-1} begins to develop approximately 2km above the ground, coinciding with an amplification of vertical velocity reaching a maximum of 15 m/s. Soon after this peak, the midlevel mini-cyclone quickly disintegrates and storm height decreases. Meanwhile, near surface vorticity rapidly intensifies to an excess of 0.05 s^-1 at 22:13 UTC which is determined to be the point which the tornado is fully developed and enters the mature stage. The near surface response to vertical vorticity and vertical velocity aloft suggests that an upward pressure gradient force was created due to a pressure anomaly created by the cyclostrophic balance associated with the strong rotation aloft. As this pressure gradient force strengthens, the existing updrafts amplifies, causing the near surface vorticity to develop via stretching

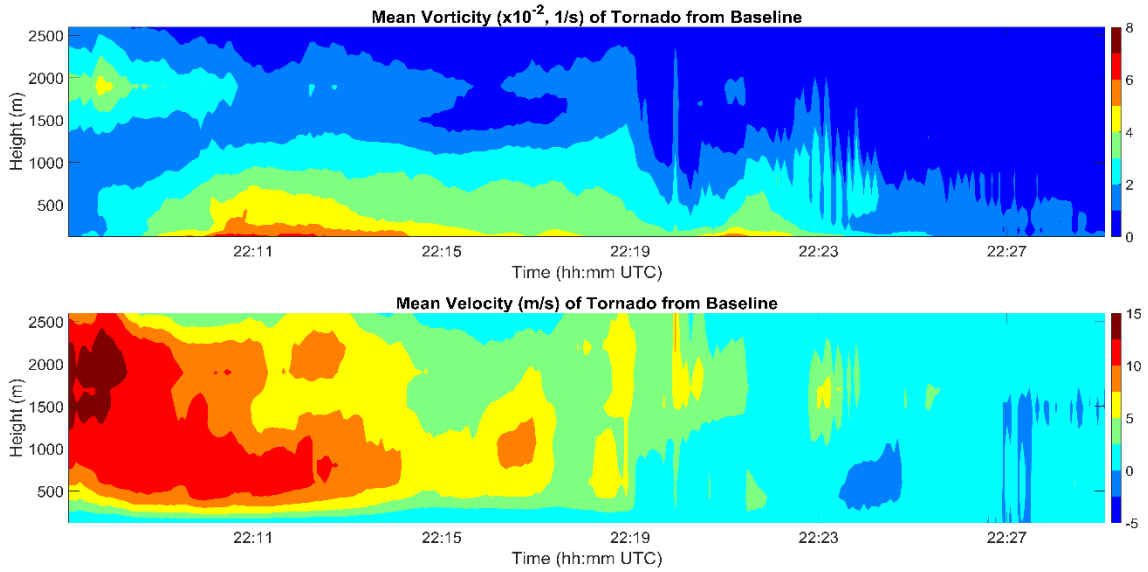

Fig. 8: Time-height evolution of vertical vorticity (1/s) and vertical velocity (m/s) averaged over an area of 333m^2 centered at the tornado.

Figure 9 shows the horizontal and vertical distribution of vertical vorticity, pressure perturbation, vertical velocity, and cloud condensate mixing ratio of the simulated tornado at 22:13 UTC. The tornado extends downward about 1.5 km toward the surface. Interestingly, the tornado possesses a mini hurricane-like structure in a sense that it includes a well-defined low-pressure eye dominated by the downdraft and an eyewall encircling the tornado eye. At 400m above ground an annulus of positive vertical vorticity and vertical velocity with three localized maximum values of vertical vorticity embedded in the annulus. The maximum horizontal winds can be found around these sub vortices. The center of the vortex is dominated by downdrafts reaching 5 m/s while the vertical velocity in the surrounding annulus maximizes at 10 m/s. The vertical cross sections display a noticeable northward tilt with height likely because the mini supercell

is embedded in an outer rainband of Hurricane Ivan. Convective cells in rainbands oftentimes contain a radially outward tilt with height as rapidly ascending air will follow isolines of angular momentum which also tilt radially outward (Hence & Houze 2008). The general structure of the tornado vortex resembles a two-cell tornado (Davies-Jones et al. 2001), a vortex with a wall of updrafts and enhanced vertical vorticity found at a distance from the tornado vortex center dominated by descending air and minimum vertical vorticity. The vertical distribution of cloud condensate associated with the tornado touches the ground, making it visible like the real tornadoes observed in TCs. The horizontal distribution of total water clearly shows a hook-shaped appendage of water condensates surrounding the north and west side of the vortex interacting with a dry air band surrounding the south and east side of the vortex. The effects of dry air intrusion on tornado formation and development will be discussed in chapter 5. Outside of the annulus there appears to be a rear flank downdraft that has wrapped around the south side of the vortex. Through the life of the tornado, this rear flank downdraft will cyclonically wrap around the tornado. The origins of this downdraft were not investigated so, a definitive conclusion about this feature cannot be drawn using this data. However, the potential importance of this feature in organizing and maintaining the tornado structure will be theorized in section 3d.

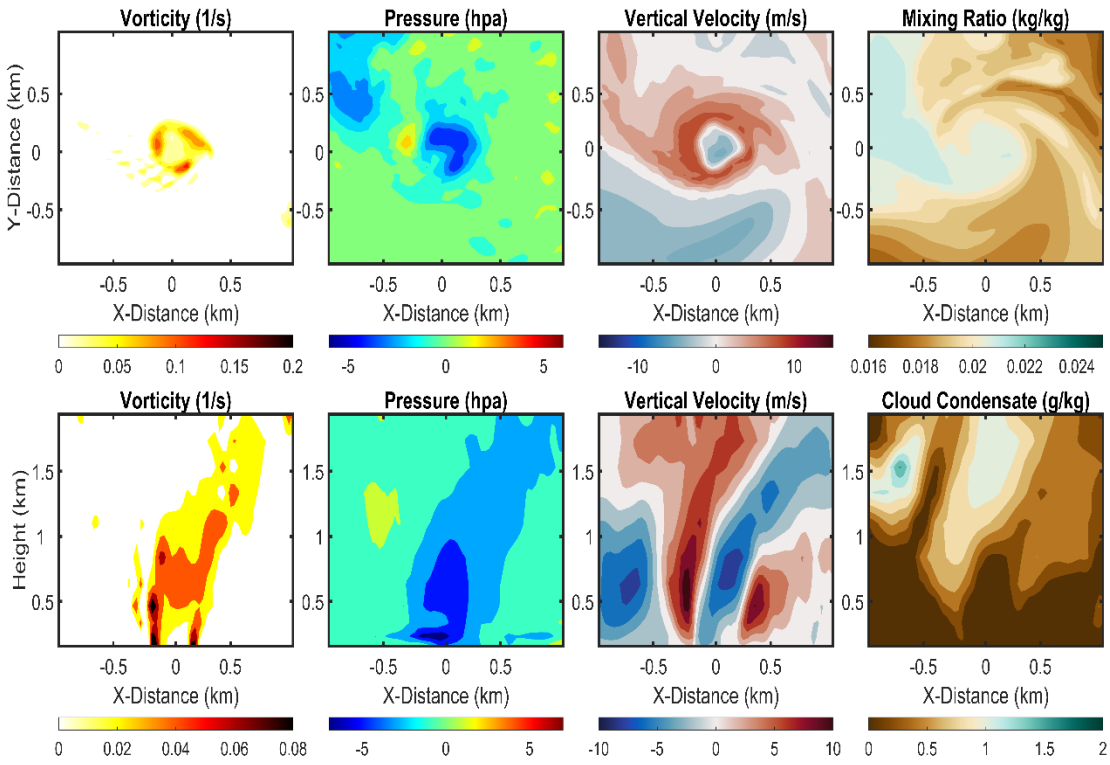

Fig. 9: Upper panels: Horizontal distribution of vertical vorticity, pressure perturbation, vertical velocity, and total water mixing ratio at 450 m above the ground of the tornado at 22:13 UTC Sept. 15. Lower panels: Vertical cross-section of vertical vorticity, pressure perturbation, vertical velocity, and cloud condensate mixing ratio at the line shown in the upper-left panel.

The three-dimensional structure of the tornado can be demonstrated using the streamlines of the perturbation winds. Figure 10 shows the 3-D structure of the baseline tornado at 22:13 UTC. The storm relative flow curls cyclonically up the vortex column from the surface, extending up to 1.5 km. The vortex once again displays an increasing northward tilt with height. The embedded subvorticies found in figure 9 cannot be distinguished in the vortex streamlines, indicating that these subvorticies are small and disappear too quickly to be discerned from the parent circulation.

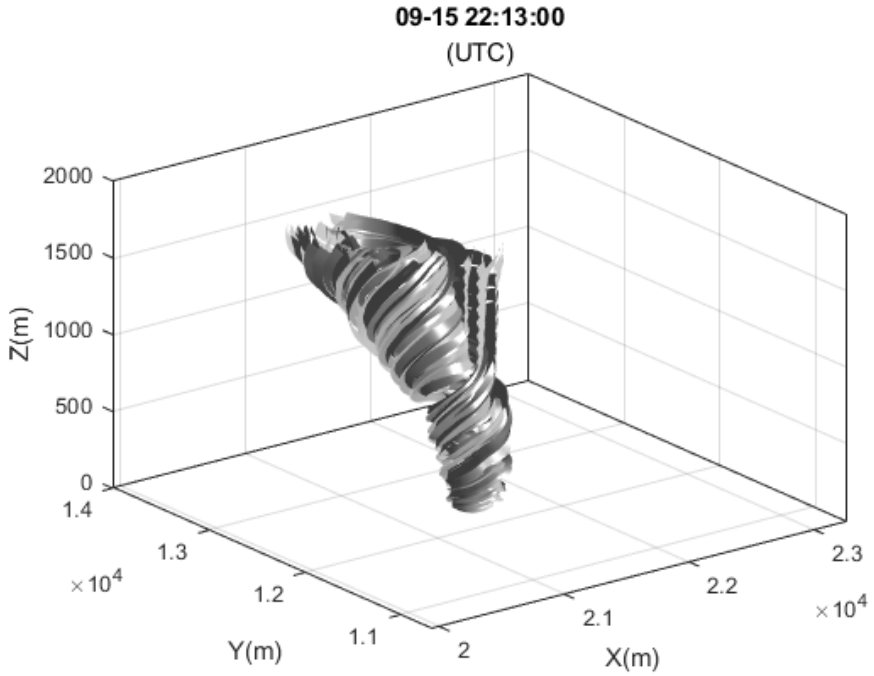

Fig. 10: 3D streamlines of the simulated baseline tornado by domain D6 at 22:13 UTC Sept. 15, 2004.

c. BASELINE TORNADOGENESIS

The generation of our simulated tornado will be carefully examined in this section. Figure 11 shows the temporal evolution of the vertical relative vorticity at 30 m above the ground resolved by domain D6. At 22:07:00 UTC the vertical vorticity is chaotic and randomly distributed across the surface. Over the next one and a half minutes the chaotic surface relative vorticities become organized into a single cell vorticity cluster with the maximum vorticity located at the center. The vortex cell continues to rapidly evolve into a structure resembling a vortex annulus 0.2 km across with a central downdraft surrounded by enhanced vertical vorticity and velocity. One minute later, a

proto tornado circulation forms at the surface. By 22:10 UTC, multiple vortices develop within the annulus and the tornado reaches its mature stage. This progression is very similar to the generation process found in midlatitude supercells. Tornadoes will transition from multiple randomly distributed vortices to a single laminar vortex core to a turbulent vortex with multiple subvortices as the swirl ratio increases. Lewellen 1962 defines the swirl ratio as the ratio of the tangential circulation of a vortex and the updraft velocity. It effectively measures the amount of mass around the circulation center and how well the mass can be evacuated vertically. If the swirl ratio reaches 2 or greater the vertical velocity is not strong enough to evacuate the mass and the circulation break down into multiple vortices.

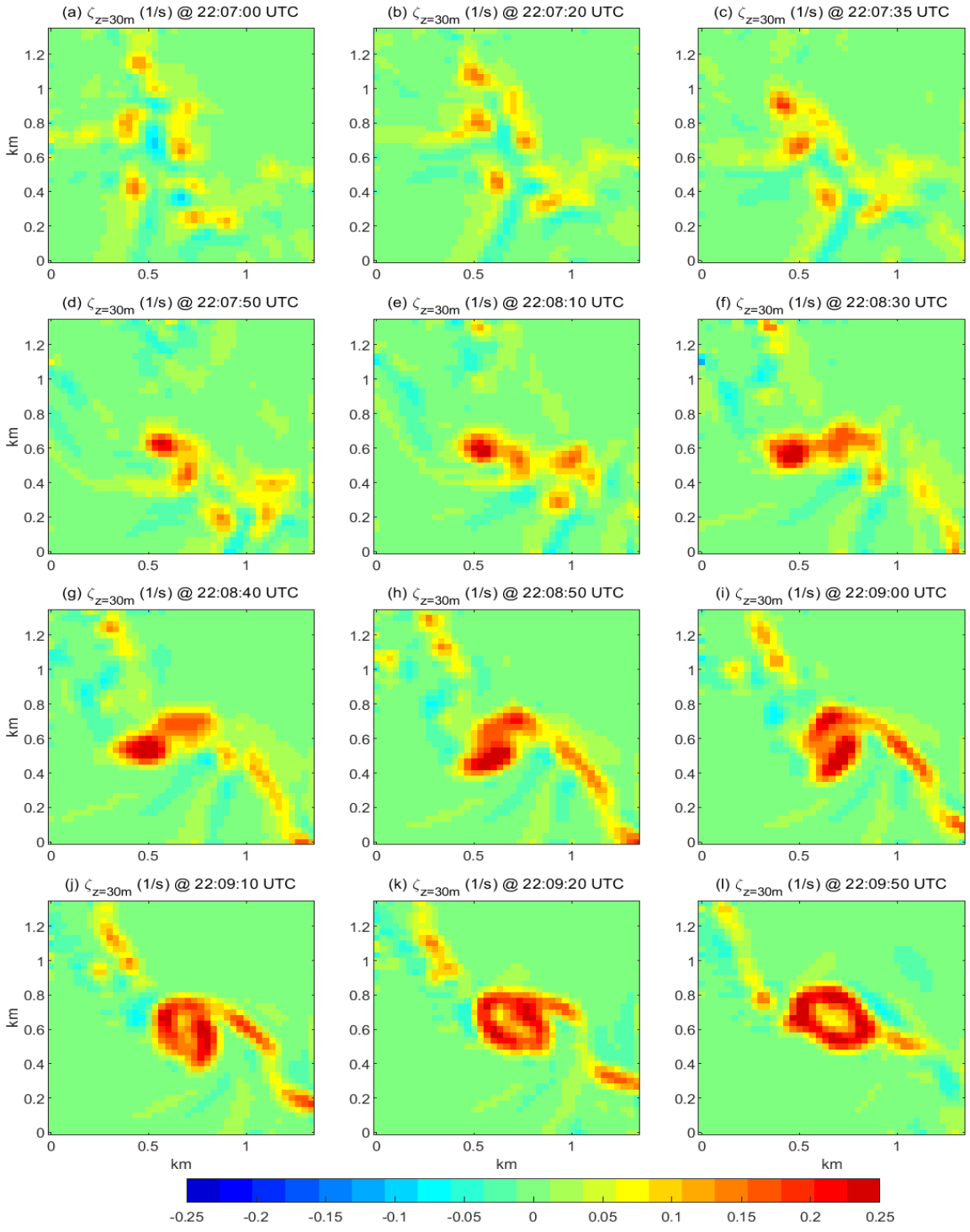

Fig 11: Vertical relative vorticity at 30 m high above the ground at the times during the genesis of a TC tornado simulated by the domain D6 of WRF-LES.

To clarify the mechanism for tornadogenesis and organization, the source and amplification process of vertical vorticity must be identified. The budget equation of vertical vorticity is depicted in Eq1. ζ is the relative vertical vorticity, *u,v, and w* are the velocity components in the *x, y,* and *z* directions in a local Cartesian coordinate; f is the planetary vorticity, ρ represents the air density; and p is the atmospheric pressure. Terms I, II, III, and on the right-hand side (RHS) of Eq. 1 represent the convergence, tilting, and the solenoidal generation of vertical vorticity, respectively. Note that the calculations were performed in the storm relative frame. Figure 12 shows the surface (z=30 m) vorticity tendency induced by convergence at the same times as figure 11. Comparisons shows that patterns by which the TC tornado vortex organizes itself closely follows the distribution patterns of the convergence term, suggesting surface convergence is the main mechanism by which cyclonic vorticity may organize and lead to tornadogenesis. In other words, surface convergence provides the main method to efficiently organize randomly distributed vorticity into the eventually tornado annulus. This explains why tornado circulation can organize very quickly.

$$\frac{\delta \varsigma}{\delta t} = -(f + \varsigma)\left(\frac{du}{dx} + \frac{dv}{dy}\right) - \left(\frac{dw}{dx}\frac{dv}{dz} - \frac{dw}{dy}\frac{du}{dz}\right) - \frac{1}{\rho^2}\left(\frac{d\rho}{dx}\frac{dp}{dy} - \frac{d\rho}{dyy}\frac{dp}{dx}\right) \qquad (1)$$

I II III

Previous studies have suggested that the tilting term, while not as potent as the convergence term, serves as the initial catalyst for vortex organization (Mashiko 2009). However, our simulation shows that the tilting term is only of secondary importance for tonadogenesis even in the early stages of development. Markowski 2010 explains that

tilting of horizontal vorticity into the vertical is an inefficient way of generating vertical vorticity. Updrafts are weak near the surface and cannot suddenly turn the horizontal tube upright, which leaves the surface void of vertical vorticity. Downdrafts from the parent circulation are usually required to transport the tilted vorticity to the surface, but mini supercells are too small and weak to provide sufficient downdrafts. While the tilting term gets stronger as vertical velocity increase with height, it is not a leading term in the vorticity budget. This is evident from the vorticity tiling at 157 m above the ground whose magnitude and shape are incomparable to the vorticity convergence. Also, system-wide tilting does not appear to be a clear mechanism for organizing the randomly distributed vorticity into a tornado circulation. Finally, the solenoidal term has negligible contribution to vorticity generation and is thus omiited.

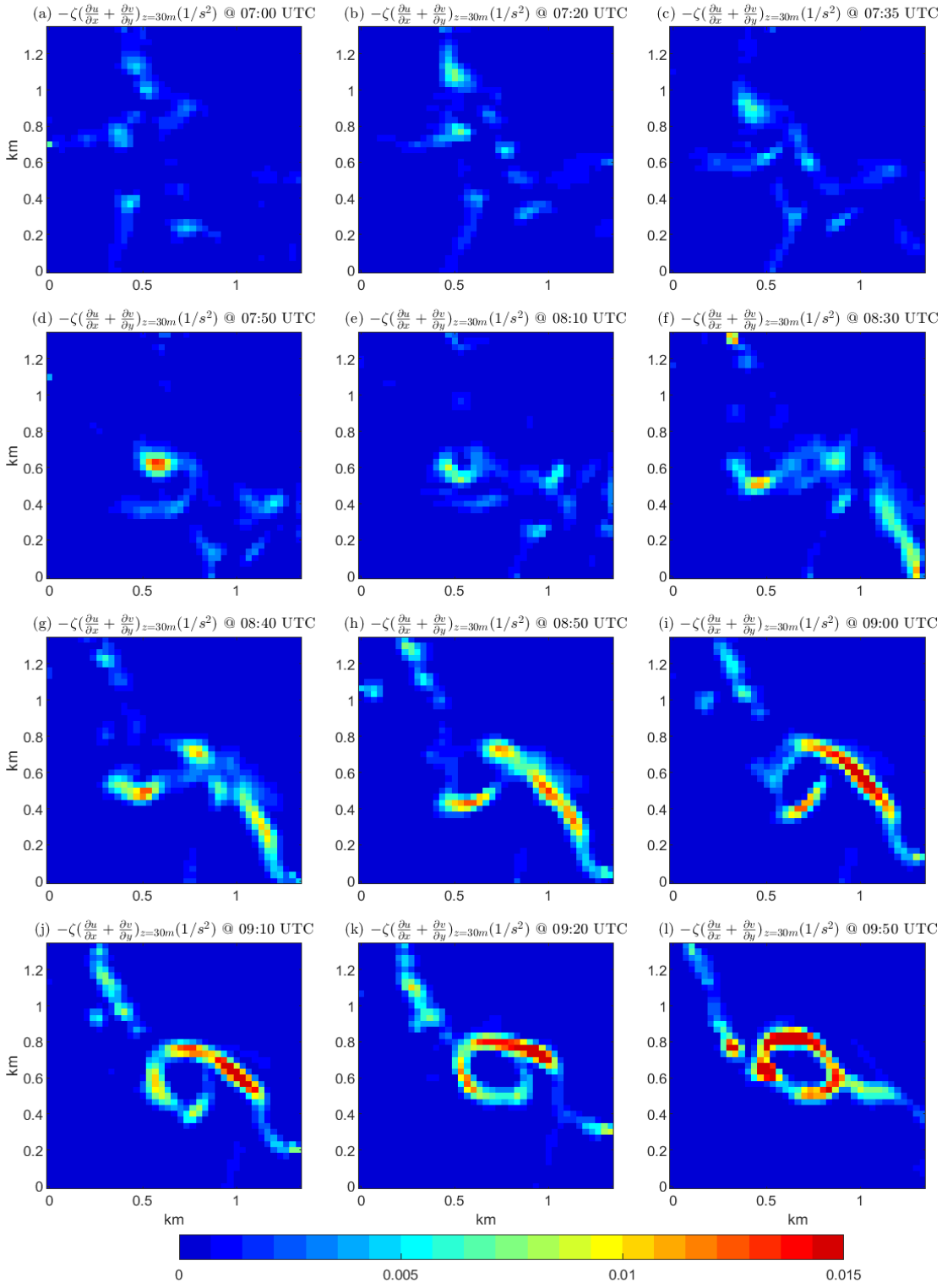

Fig. 12: Vorticity tendency induced by convergence at 30 m high above the ground at the same times as those in Fig. 11.

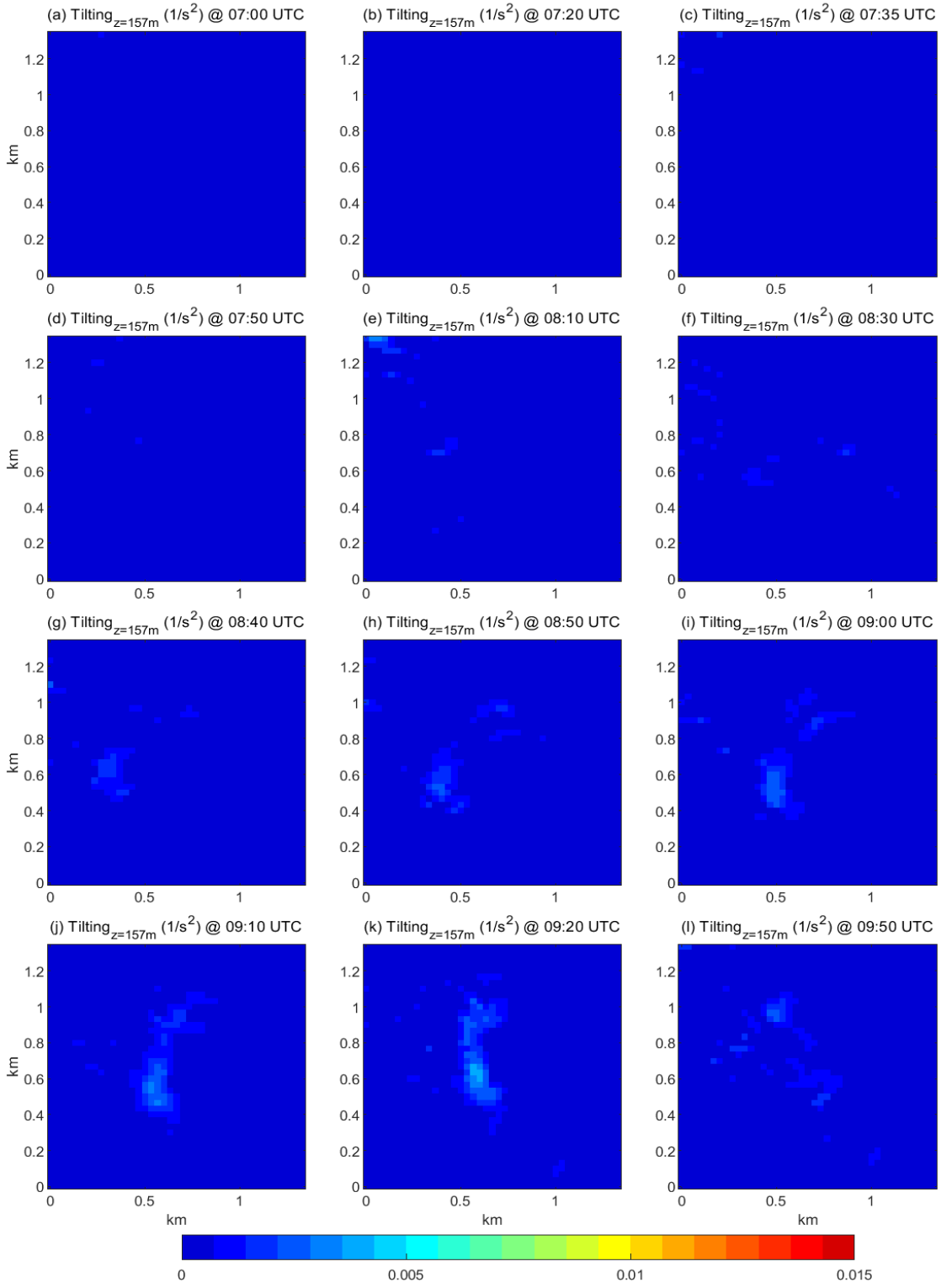

Fig. 13: Vorticity tendency induced by vertical tilting at 157 m high above the ground at the same times as those in Fig. 11.

The importance of surface convergence in tornado formation may also explain why tornadoes tend to form at the outer rainbands where convergence is strongest. Figure 14 shows that strong convergence more than-0.08 s^{-1} exists in the same rainband where our baseline tornado formed. Areas of strong surface convergence can be observed by forecasters or predicted by numerical models ahead of time, meaning the location of TC tornadoes could be forecasted to a higher degree of accuracy.

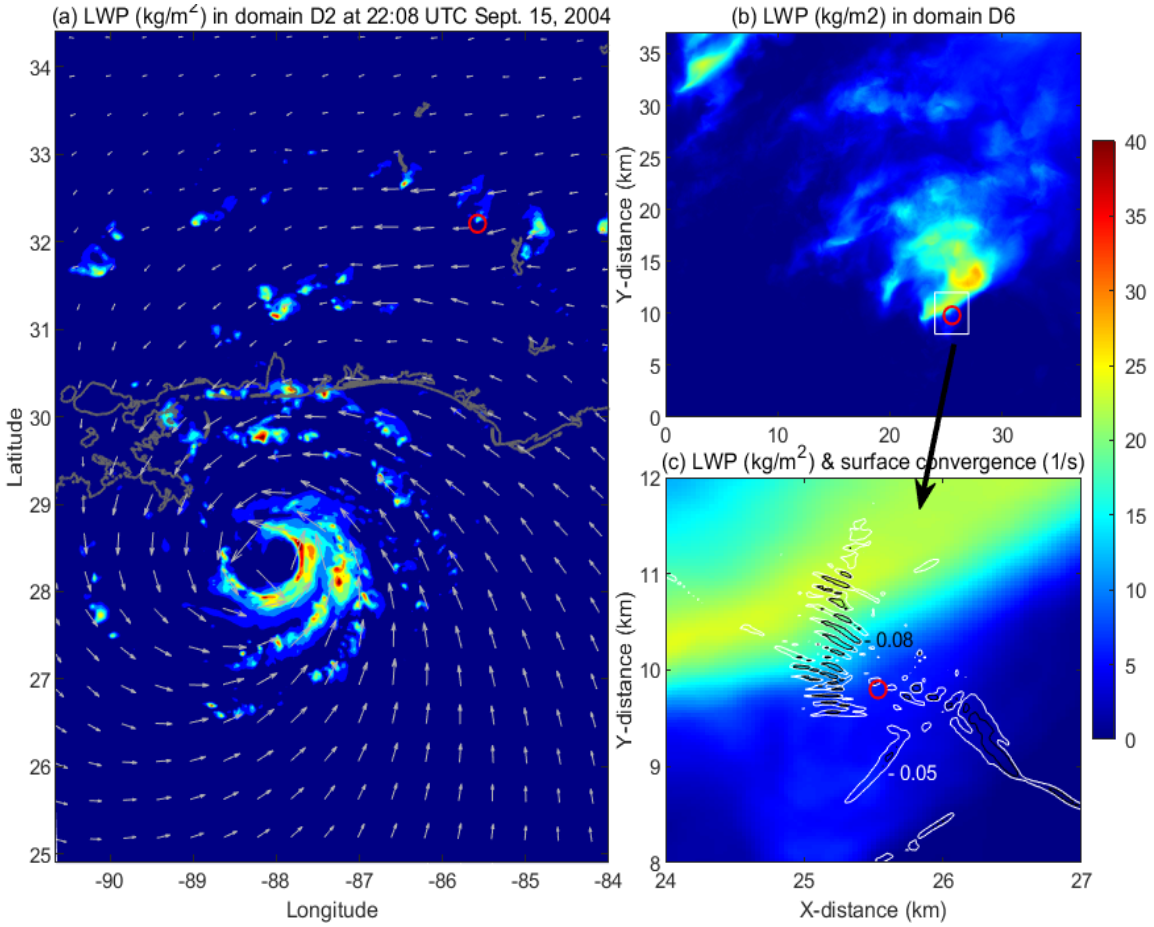

Fig. 14: (a) Liquid water path (LWP, kg/m^2) and surface winds of Ivan (2004) simulated by domain D2 at 22:08 UTC on Sept. 22, 2004. Red circle indicates the location where a TC tornado forms. (b) LWP in domain D6. (c): Zoom-in plot of LWP and surface convergence (white contours: -0.05 s^{-1} and black contours: -0.08 s^{-1}) in the white box in (b).

d. BASELINE TORNADO DISSIPATION

This section will investigate the dissipation process of the TC tornado. It was just established in the previous section that the formation of a tornado is dependent on the location of surface convergence. Should a feature cut a tornado from sources of surface convergence, the tornado may dissipate. Figure 15 depicts the vertical velocity at end stages of the tornado lifecycle overlaid with areas of strong surface convergence. The rear flank downdraft mentioned earlier is present at the southside of the tornado vortex. At the peak of tornado maturity, the tornado has prominent sources of surface convergence in the east and west side of the vortex. However, as the rear flank downdraft wraps cyclonically around the tornado vortex it effectively cuts off the eastern sources of weakens before breaking apart and mixing with the downdraft air. In a sense this process also dissipates tornadoes in the midlatitudes, however it does not explain why most TC tornadoes dissipate quicker than traditional tornadoes. I propose a secondary mechanism may contribute to the collapse of the TC tornado, barotropic instability.

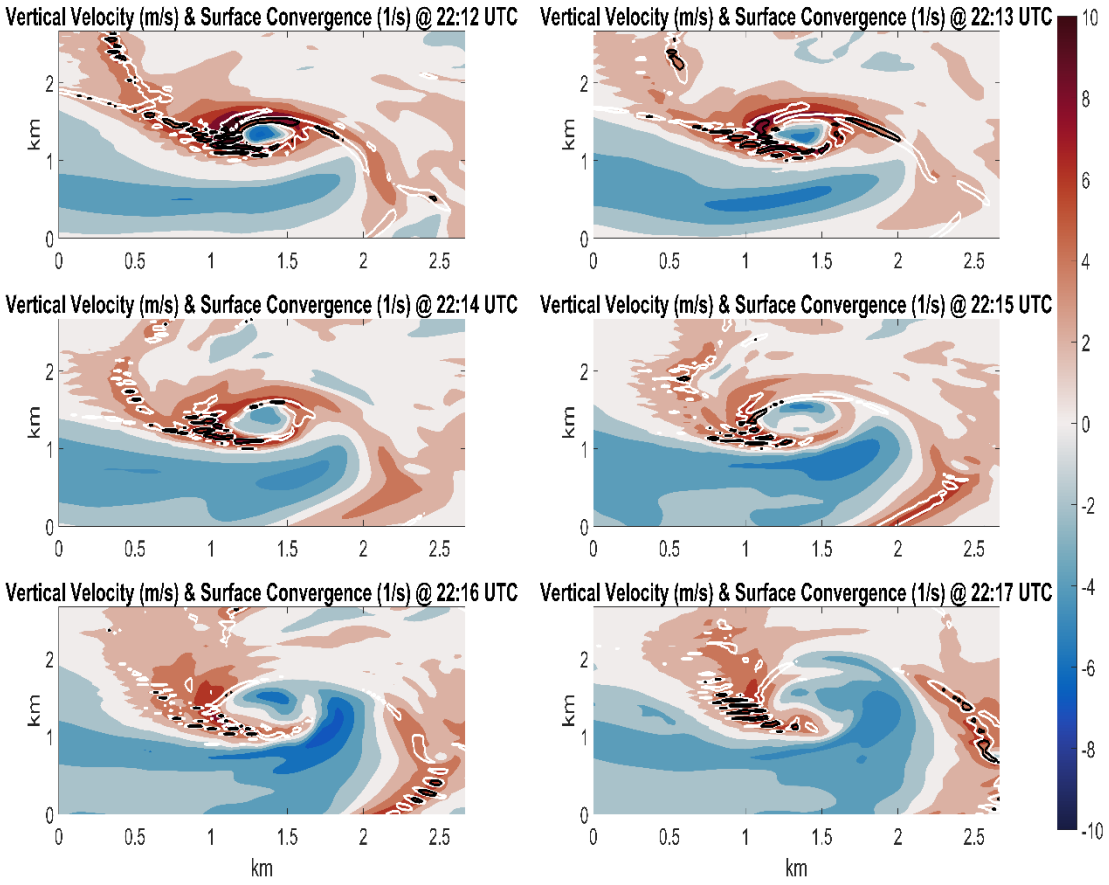

Fig. 15: Vertical Velocity (color shade) and surface convergence (contour) at multiple times during the decay of the TC tornado simulated by WRF domain D6

Recall that our tornado vortex structure resembles a vortex annulus with embedded subvorticies. Figure 16 a) depicts the vertical vorticity captured at 22:13 UTC overlaid with the tornado circulation. Shubbert et al. 1999 describes a vortex annulus as the result of opposing vorticity gradients on the opposite sides of the annulus leading to barotropic instability. Barotropic instability allows the embedded subvorticies to grow to fully sustained eddies. By removing the azimuthal-mean tangential wind we can observe

the small-scale eddies embedded in the rotation. Some of the eddies rotate in the opposite direction of the tornado circulation. Embedded subvorticies can dissipate a tornado in two ways, by drawing kinetic energy from the tornado circulation weakening the circulation, and by distorting the tornado structure shape and causing it to tear apart. Figure 17 shows the relative vertical vorticity captured at a 30m height towards the end of the simulation. At 22:13, the tornado peak, the vortex structure resembles a small vortex annulus with embedded subvorticies, but by 22:15 UTC the vortex doubles in size and has become increasingly disorganized. By 22:16 UTC the tornado vortex has broken apart and begins to dissipate. Both the disconnection of surface convergence and barotropic vorticity may work in tandem to dissipate TC tornadoes at a quicker rate than midlatitude tornadoes. A further analysis will analyze the dissipation methods in greater detail and will be the subject of a future study.

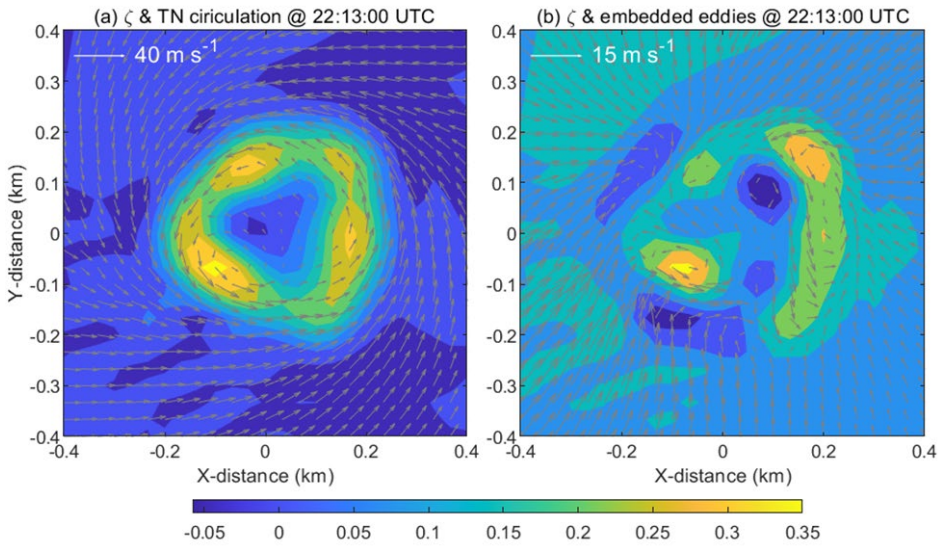

Fig 16: *(a) Relative vorticity annulus and wind vectors at 30 m above the ground of the simulated tornado at 22:13:00 UTC on Sept. 15, 2004. (b): The same as (a) but with the azimuthal-mean tangential wind and relative vorticity of the tornado removed.*

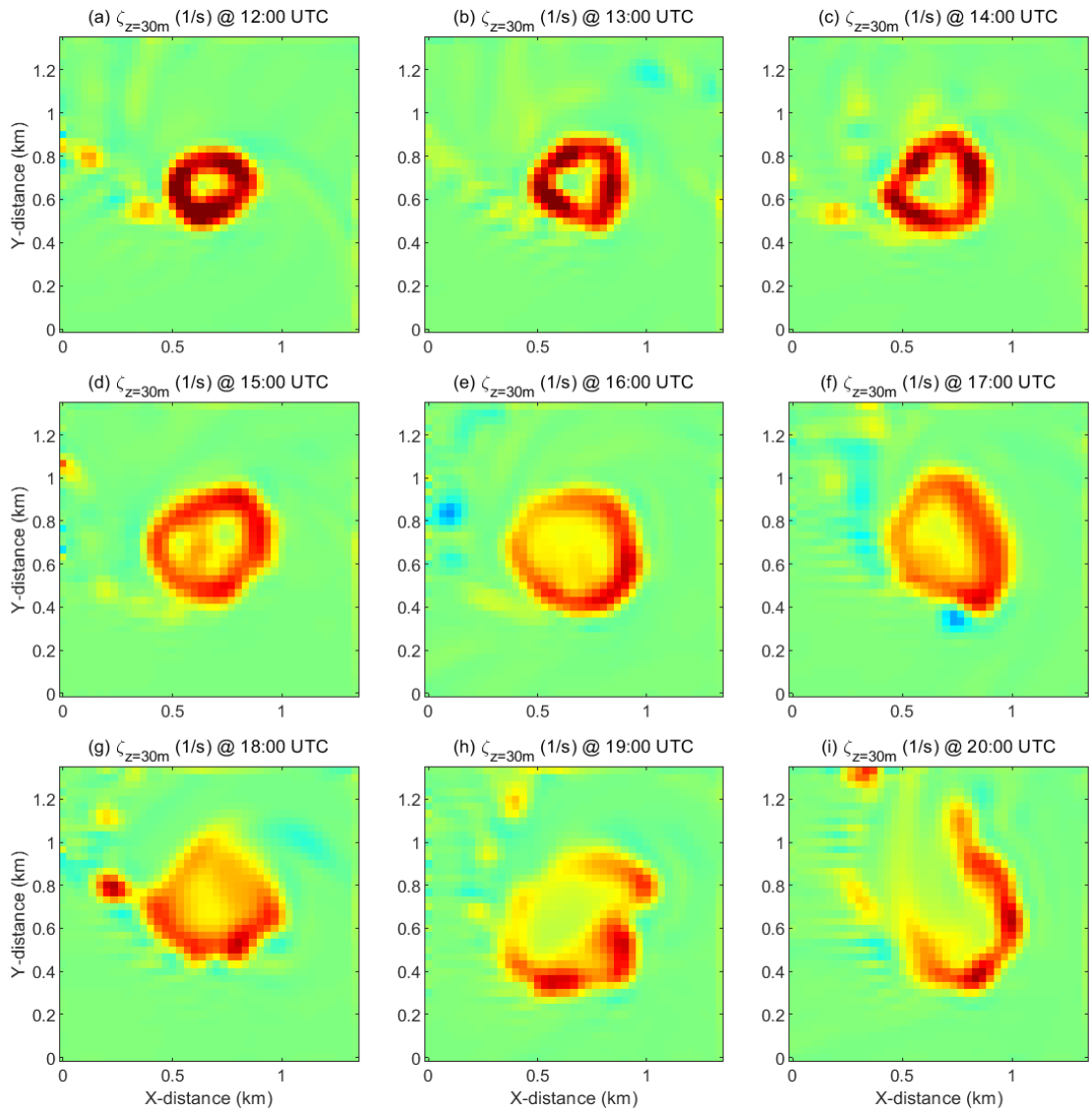

Fig. 17: Relative vorticity at 30 m above the ground of the simulated TC tornado at different times toward the end of the tornado lifecycle.

Chapter 4 TSK+2 RESULTS

a) TSK+2 ENVIRONMENTAL FIELD

In the first sensitivity experiment, the surface skin temperature is raised two degrees prior to tornado formation so that the tornado may form under slightly higher convective instability without changing the environmental lapse rates above. This was done by artificially increasing the land surface skin temperature in domain D6 by 2 degrees once the Noah land surface model determined the land category. As a result, the hydrometeor distribution of Hurricane Ivan and tornado location of our sensitivity experiments would remain similar throughout. The sensitivity experiment does allow us to observe any changes to the time of tornado formation and any structural changes that the tornado may undergo. In the new TSK+2 experiment run, the average CAPE value in domain d6 was 50 J/kg higher than the baseline run (not shown), though some locations experienced CAPE 200 J/kg higher than the baseline. A simulated thermodynamic sounding of the TSK+2 rainband in proximity of the tornado found that the surface-based CAPE is approximately 2389.4 J/kg, significantly higher than our baseline experiment (figure 18). However, the 0-1 km shear and 0-1 km SRH are similar to the baseline and the evidence of dry air intrusion remains, allowing us to conduct our sensitivity experiment.

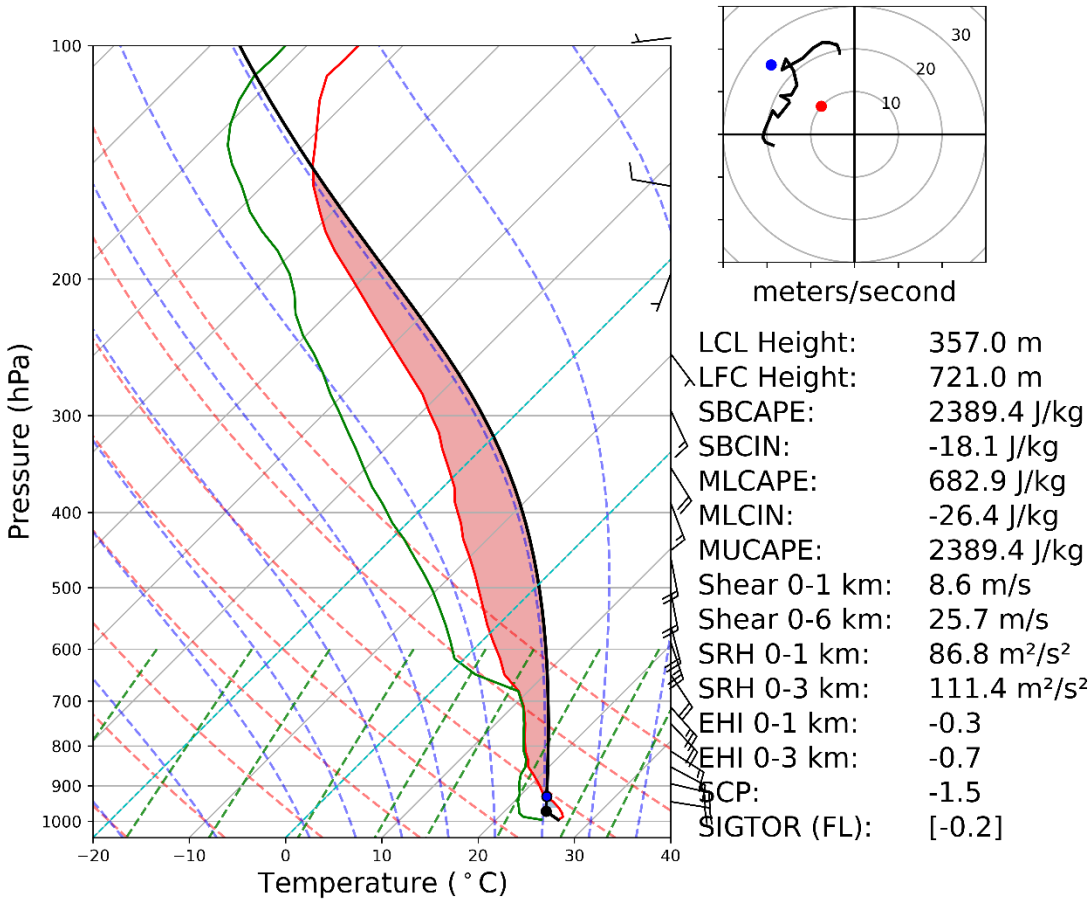

Fig. 18: Simulated SkewT-logp and hodograph analysis sounding of Hurricane Ivan at 22:13 UTC Sept. 15, 2004. The red line is temperature, the green line is dew point, and red shading is the lowest 100-mb mixed layer CAPE. Hodograph depicts the shear magnitude from 0–6-kilometer heights. Red (blue) dots represent the Bunker's right (left) storm relative motion

b) TSK+2 TORNADO STRUCTURE

Figure 19 shows that the time height cross section of the mean vertical vorticity and vertical velocity averaged 333X333 m surrounding the TSK+2 tornado. While appearing very similar to the baseline cyclone, the TSK+2 persisted for a longer time. The vorticity structure aloft remains unchanged with a max vorticity of 0.03 1/s located at 2000 meters above the ground. Vorticity at the lower levels degrade at a much slower rate

than the baseline allowing the tornado to remain organized even at times when the baseline has undergone collapse. The TSK+2 tornado also does not undergo a unilateral collapse at all levels like the baseline, instead the vortex becomes disconnected from the surface, but the tornado remains organized for a time and even attempts to reconnect with the ground before undergoing a full collapse by 22:23 UTC. Interestingly, despite the greater convective instability, there are only marginal differences in the mean vertical velocities between both experiments. In fact, the only times when the TSK+2 experiment had greater vertical velocity than the baseline was toward the end of the simulation when the baseline tornado had already dissipated.

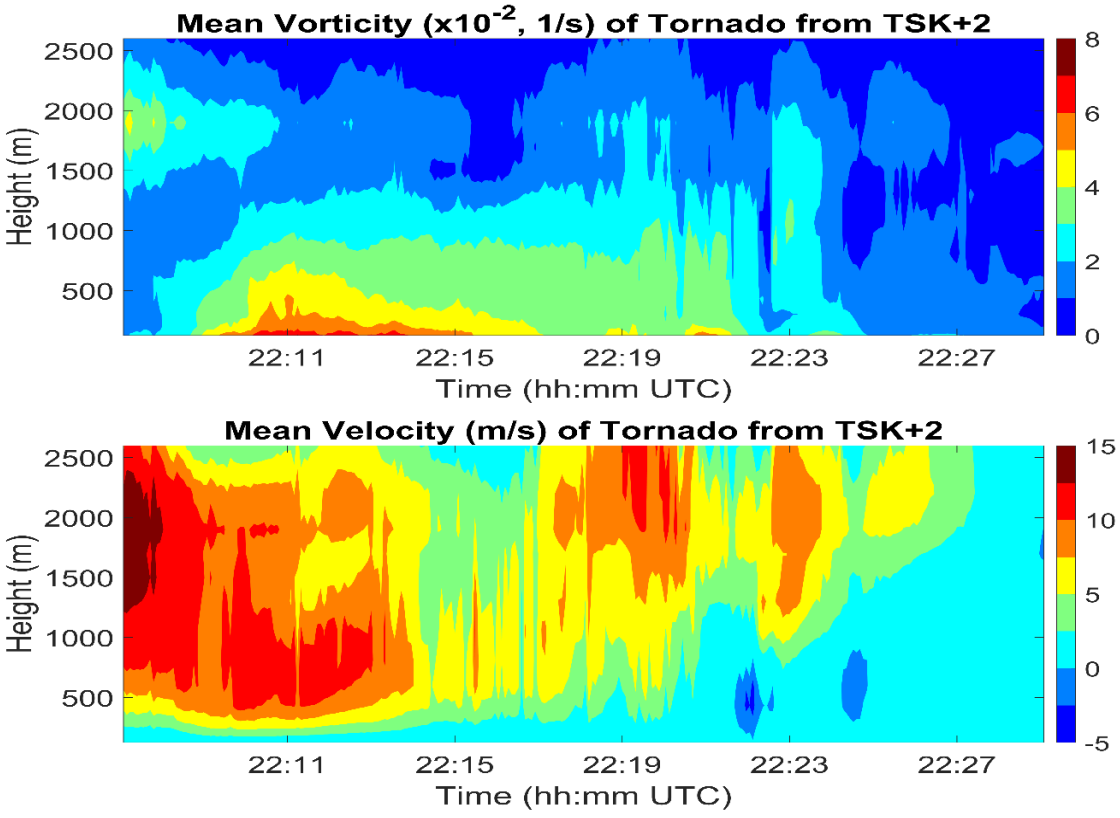

Fig. 19: Time-height evolution of vertical vorticity (1/s) and vertical velocity (m/s) averaged over an area of 333m^2 centered at the TSK +2 tornado.

Figure 20 depicts the horizontal and vertical convective environment at the same time as figure 9. Both tornadoes are at mature stages and exhibited many similar properties. The vertical vorticity at 450m above the ground feature the same annulus shape as the baseline run, but the annulus is more axisymmetric in the TSK+2 run than in the baseline. The subvorticies found in the TSK+2 run is weaker but more plentiful than the baseline run. The pressure fields between both runs are equal in magnitude and the TSK+2 run having a more axisymmetric shape than the baseline. The vertical velocity fields in the two runs display the same hurricane eye-like structure with equal max updraft velocities of 15 m/s, flanking a central downdraft of approximately 7 m/s. The TSK+2 experiment contains slightly higher vorticity aloft, maximizing at 0.06 1/s, but contains a similar vorticity distribution as the baseline.

Figure 21 depicts the 3-D structure of the TSK+2 tornado at 22:18:05 UTC. The tornado structure is similar to the baseline tornado, extending to 1.5 km above the ground and still containing the northward tilt with height. However, the tornado appears to be disconnected form the ground but does not undergo collapse. Instead for the next several minutes the tornado remains organized aloft.

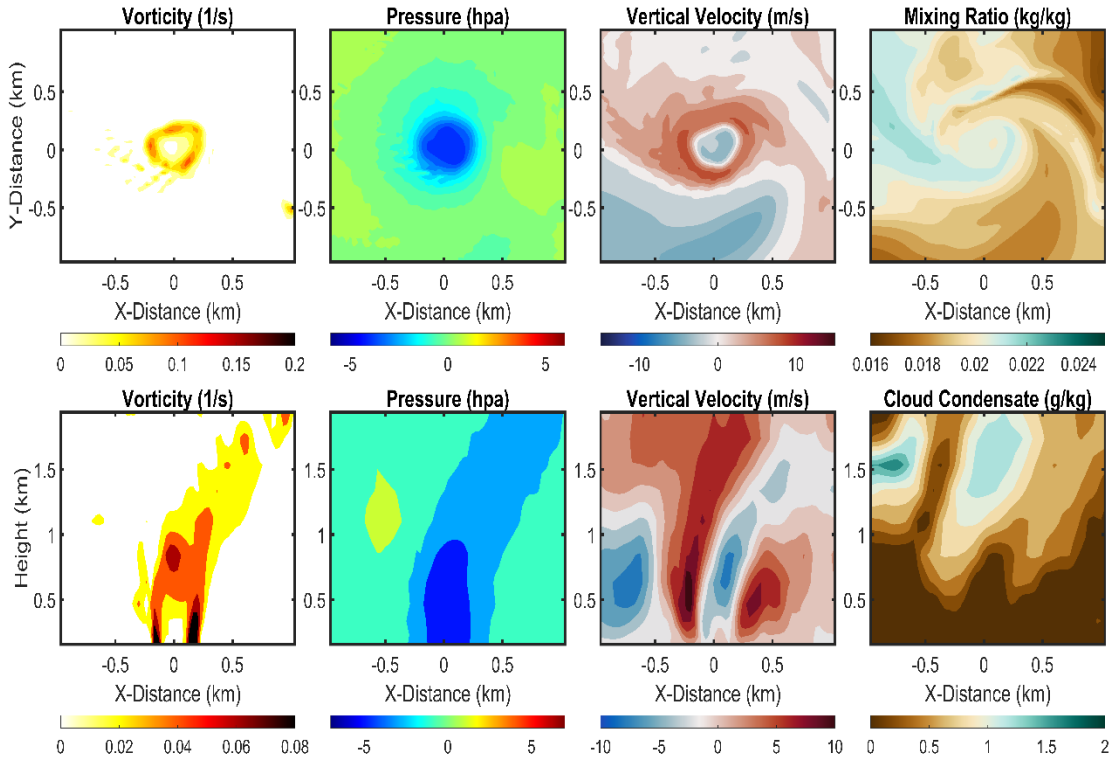

Fig. 20: Same as Figure 10 but for TSK+2 experiment

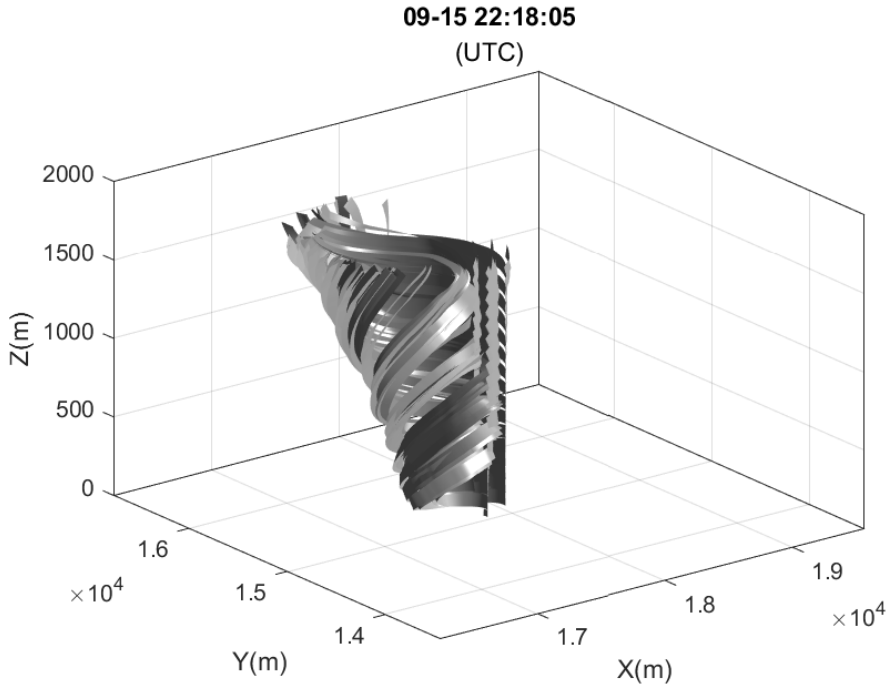

Fig. 21: 3D streamlines of the simulated baseline tornado by domain D6 at 22:18 UTC Sept. 15, 2004.

Results from figures 19-21 suggests that the increased convective instability does not appear to enhance the strength and change the structure of the tornado but allows the tornado to persist longer. A similar vorticity budget analysis was conducted for the TSK+2 tornado (not shown) and the results were identical to the baseline, the highest contribution to vertical vorticity was convergence followed by marginal contribution from tilting terms and negligible contribution from the solenoidal terms. The dissipation of the TSK+2 tornado resulted from a disconnection of surface convergence and baroclinic instability. These results stand in contrast to previous numerical simulations of TC tornadoes. Carrol-Smith et al. (2021) numerically simulated Hurricane Ivan and the possible TC tornado development under different future climate scenarios to examine if TC tornado behavior will change under different climate forcings. Their simulations show that the sensitivity tests with higher CAPE than the current environment produce stronger updrafts and more significant rotation of mini-vortices. But fewer tornadoes were produced in the sensitivity runs with higher CAPE than in the control run under the current climate. However, the grid resolutions used in their simulations were too coarse to resolve the tornado structure like our simulations. Thus, their study only suggests a potential for producing stronger tornadoes with higher CAPEs. But this potential might not be realized as the tornado genesis is affected by other processes, which are not resolved in simulations with coarse grid resolution. One robust signal is that higher instability does allow a vortex to sustain longer

Chapter 5 RH+ RESULTS

a) RH+ ENVIRONMENTAL FIELD

As shown in Figures 9 and 20, a band of dry air wraps around the southern and eastern side of the vortex suggesting there may have been dry air intrusion affecting the TC tornado. The second sensitivity experiment is, thus, designed to examine how the intensity and structure of the tornado respond to the changes in mid-level moisture. To do so, I artificially increase RH to 80% for anywhere it is below 80% in the layer of 300 – 700 hPa in the restart file saved before the tornado forms. Conducting this experiment reduce the possible effect of mid-level dry air intrusion on tornado formation and intensification while keeping a plausible tornadic environment**.** Figure 22 shows the new SkewT-logp diagram at the same time and location as figure 7. The dry air intrusion in the baseline disappears and the entire vertical column is saturated. The RH+ environment featured a surface-based CAPE of 1814.5 J/kg and surface-based CIN of – 31.9 J/kg, which is like the thermodynamically more stable than the baseline test. The RH+ environment however featured similar kinematic properties from the baseline with 0-1 km SRH of 85.7 m^2/s^2 and 0-1 km VWS of 8.3 m/s. There is also evidence of severely reduced fry air in the atmospheric column. Overall, the kinematic and thermodynamic properties found in this experiment seems slightly less conducive for tornado production than the baseline experiment, but all derived values are within tolerable variance from the baseline, allowing us to conduct out sensitivity experiment.

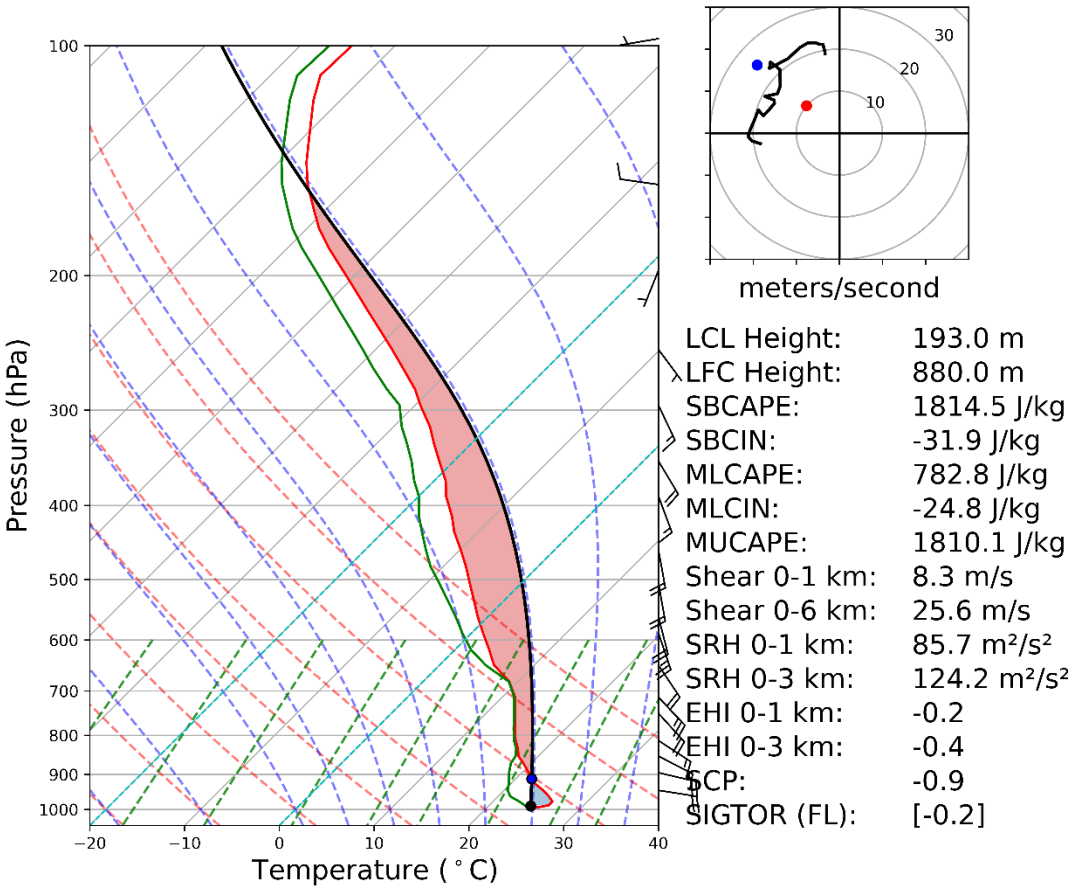

Fig. 22: Simulated SkewT-logp and hodograph analysis sounding of Hurricane Ivan at 20:13 UTC, 15 September 2004 but for the RH+ experiment. The Red line is temperature, The green line is dew point, and red shading is the lowest 100-mb mixed layer CAPE. The black line in the hodograph represents the 0-6 km shear magnitude. The red (blue) dots represent the Bunker's approximate right(left) storm motion

b) RH+ TORNADO STRUCTURE

Figure 23 depicts the time-height plot of the mean vertical vorticity and mean vertical velocity of the RH+ test. While the evolution of vorticity and vertical velocity of the simulated tornado in the two simulations is similar, there are noticeable differences. Firstly, the mini-cyclone in the RH+ experiment takes slightly longer to reach its maximum vorticity compared to that in the baseline simulation. In the initial stage, the

near ground vorticity in the RH+ run quickly reaches the maximum mean vorticity of more than 0.05 1/s, which has a more explosive growth rate than that of the baseline simulation. The maximized vorticity in the RH+ run reaches a greater height of nearly 500 m, compared to the height of merely 250 m in the baseline simulation. The vertical velocity in the RH+ experiment was much stronger than the baseline, achieving a max value of 13 m/s a greater height than the baseline. Although the initial growth was more extensive in the moister environment, the mini-vortex dissipates quicker than that in the baseline simulation. By 22:20 the entire near-surface vortex structure has dissipated, leaving zero vertical vorticity from ground level to 1.5 km. Interestingly, at 22:23 UTC a second mini-cyclone develops aloft in the same location as the first dissipated. The second mini-cyclone does not last long and dissipates by 22:23 UTC. These results came somewhat as a surprise. With the removal of dry air aloft, we expected a suppression of downdraft development. However, not only was there no downdraft suppression, but the environment was primed for a second tornadic reorganization.

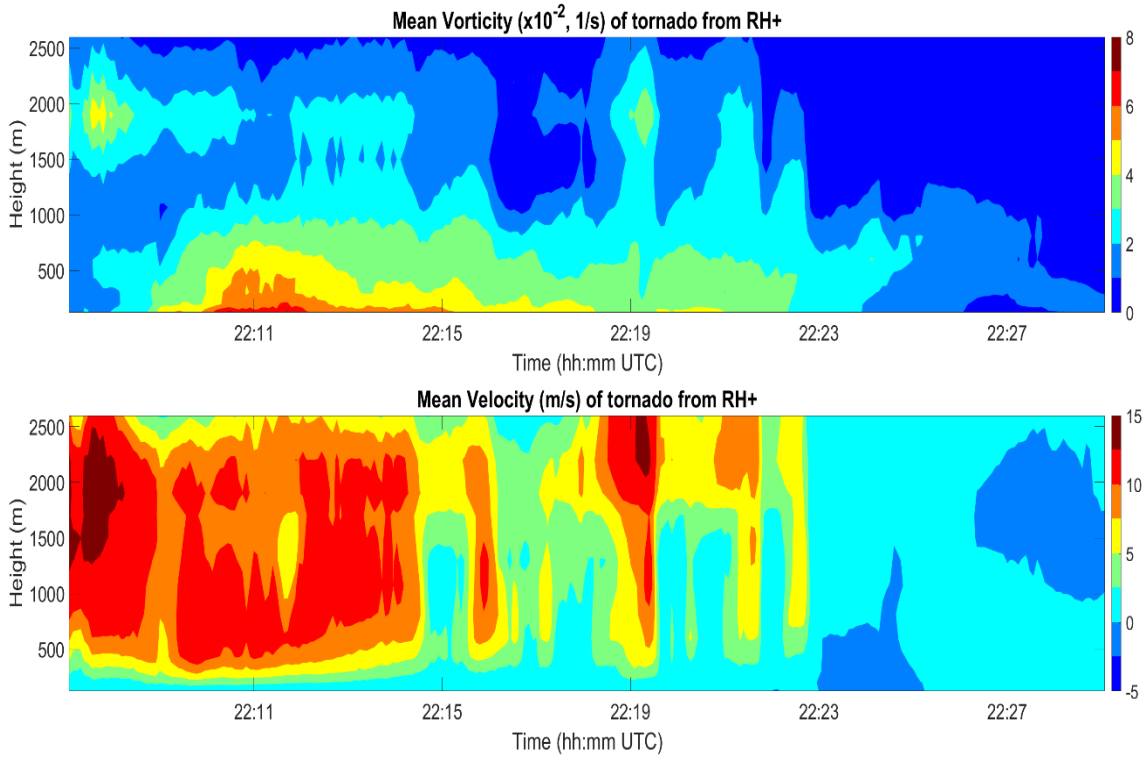

Fig. 23: Same as Figure 8 but for RH+ experiment

Figure 24 shows the horizontal and vertical cross-section of the simulated tornado and its environment from the RH+ experiment at 22:13 UTC. The first interesting note was that diameter of the mini-vortex was approximately 20% smaller than the baseline experiment. However, the RH+ tornado has a similar structure to our baseline. The vortex annulus at 450m above the ground resembles a vortex annulus with embedded vortices, though the subvorticies are more plentiful in the RH+ run versus the baseline. The vertical velocity fields reveal that there were no changes in downdraft velocity. Once again, a vertical vorticity budget was conducted on the RH+ tornado and the mechanisms for tornado genesis and dissipation remain the same. Figure 25 does reveal how the dissipation of the RH+ tornado slightly differs from the baseline test. From 22:12 to 22:19 UTC the tornado structure undergoes degradation in similar fashion

to the baseline test, doubling in size by 22:15 UTC before falling apart in 22:17 UTC. However, at 22:19 UTC the open vortex band convergences at the tip and forms a vortex cluster by 22:20 UTC giving the tornado a second life.

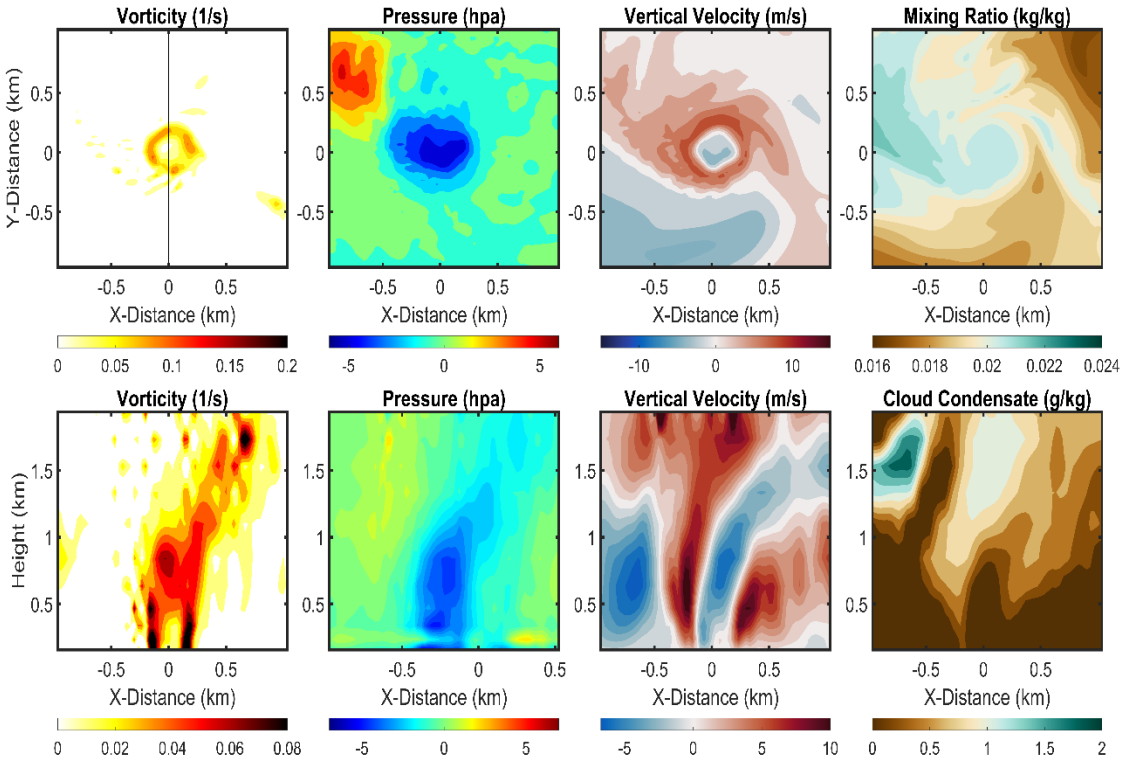

Fig. 24: Same as Figure 9 but for RH+ experiment.

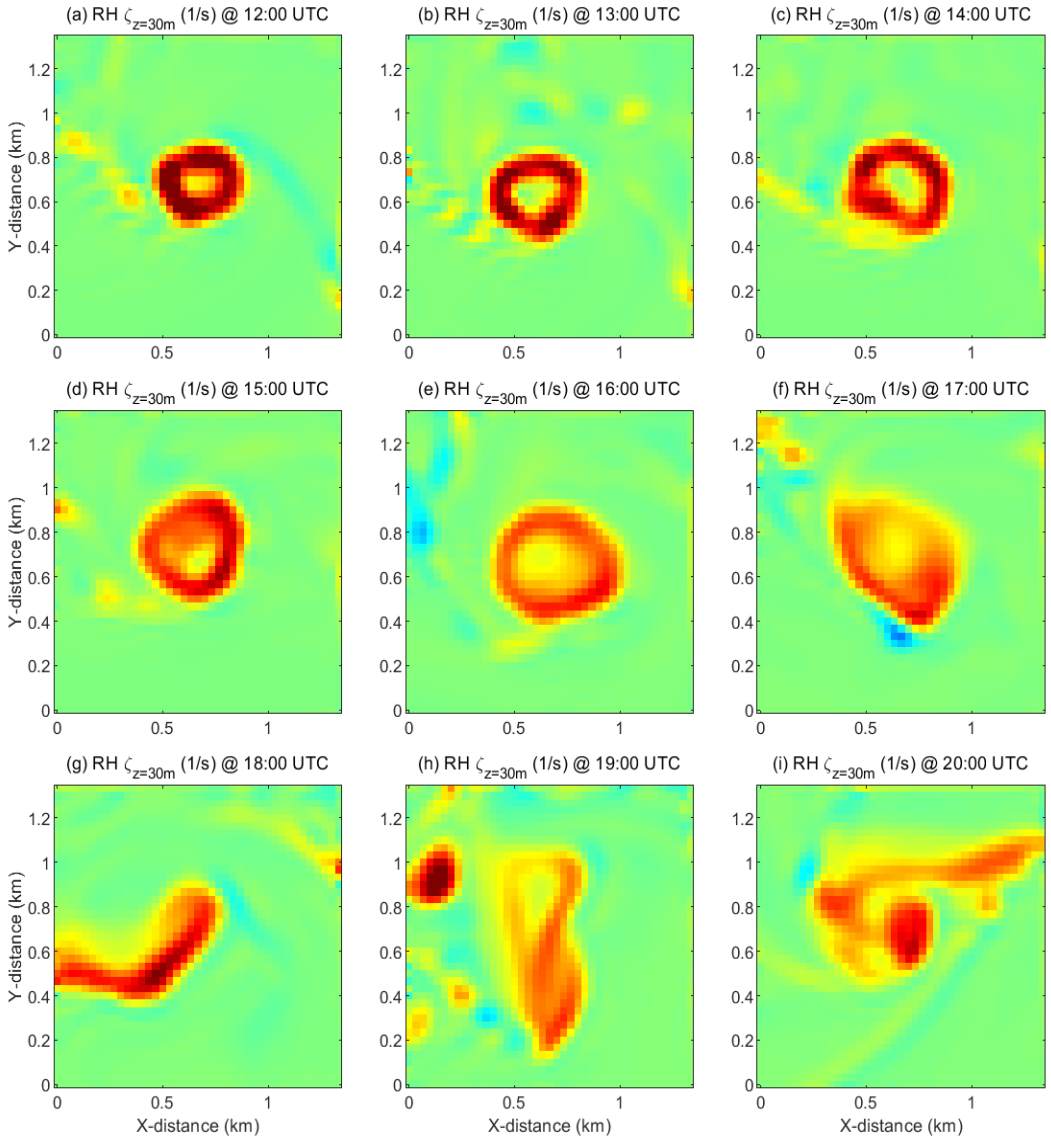

Fig. 24: Relative vorticity at 30 m above the ground of the simulated TC tornado at different times toward the end of the RH+ tornado lifecycle.

CHAPTER 6

DISCUSSION & CONCLUSION

In this thesis study, the multi-scale WRF simulations of Hurricane Ivan (2004) are used to investigate TC tornado formation, development, and the impact of environmental conditions on TC tornado intensification and structural change in a hindcasting mode. This multi two-way nested WRF simulation features an LES domain with a grid resolution of 33.3 m, the highest resolution to date for simulating TC tornadoes. This numerical system allows tornadoes, supercells that spawn tornadoes, parent rainband convection, and TC circulation to be realistically simulated in one unified system. Three numerical experiments are conducted using the WRF-LES. These include a control run, which is initialized and forced by the NFL reanalysis data, and two sensitivity experiments in which environmental conditions are changed. In the first sensitivity experiment, the surface skin temperature predicted by the Noah land surface model is artificially increased by 2 degrees, allowing us to increase the convective instability without modifying the environmental lapse rate. In the second sensitivity experiment, RH is increased to 80% for anywhere in the 300 – 700 hPa layer with RH smaller than 80%. This increased moisture reduces the possible mid-level dry air intrusion. The output of these three numerical experiments is analyzed to document the tornado structure and formation mechanisms and their response to the changes in the environmental field.

The control simulation successfully simulated an inland tornado that formed in Hurricane Ivan's outer rainband. The timing and location of the tornado formed in the outer rainband of Hurricane Ivan are consistent with observations. The rainband was located in the northeast quadrant of Hurricane Ivan and on the periphery of a large dry air

intrusion. A mid-level vortex 2 km above ground causes near-surface vorticity to stretch to a height of 1km and intensify rapidly. The tornado had measured 30 m/s winds and lasted for 15 minutes before the mini-cyclone collapsed. The tornado exhibits a hurricane eye-like structure, with downdrafts being immediately flanked by updrafts. The higher resolution of our model revealed that the tornado structure resembles a vortex annulus with embedded subvorticies. Moisture fields reveal that a band of dry air wrapped around the south and east side of the vortex, evidencing that the tornado was under the influence of the dry air intrusion. A vorticity budget reveals that convergence is the main mechanism the TC tornado uses to turn chaotically distributed vertical vorticity into a vortex annulus before becoming an EF0 tornado. These results suggest that strong surface convergence zones are prone to tornadogenesis and could potentially be forecast ahead of time. Disconnection from surface convergence and barotropic instability may have led to the speedy demise of the tornado and could explain why TC tornadoes dissipate faster than midlatitude cases.

Relative to the baseline simulation, when the surface skin temperature was raised by 2 degrees, the CAPE values, on average, went up 50 J/kg. Despite the greater convective instability the TSK+2 tornado had similar strength and structure as the baseline run, though it remained organized longer. The tornado generation and dissipation process remained unchanged in the TSK+2 run. These results stand in contrast to simulations conducted by Caroll-Smith (2021) who found that greater CAPE at landfall would produce stronger rotating updrafts. It should be noted that the contrast of my results to previous studies is likely caused by the different model grid resolution used by the two numerical studies. The tornado resolving grid resolution in my simulations

allows for a direct link between tornado itself and the environmental CAPE, whereas the coarse grid resolution used by Caroll-Smith (2021) only simulates a potential for generating tornadoes but not the tornado itself. This resolution dependent relationship between CAPE and tornadoes will be further explored in my future study.

The second sensitivity experiment shows that the reduced mid-level dry air intrusion only has a marginal impact on the intensity and structure of the simulated tornado. The tornado structure featured a smaller, shorter-lived tornado with marginal changes to intensity. The absence of dry air did suppress downdraft velocity somewhat, but a vortex was still capable of forming while utilizing the same mechanisms found in previous experiments. Even after the dissipation of the TC tornado, the environment was capable of producing another TC mini-cyclone aloft that had potential to form a second tornado. This came somewhat as a surprise. Maybe the uniformly increased moisture in the sensitivity experiment may have oversimplified the impacts of mid-level dry air on tornado development. Further study is needed to investigate the effects of varying dry air on TC tornado production and evolution.

Finally, it is important to note that this study is not meant to make a one-to-one replication of tornadoes formed in Hurricane Ivan. Instead, the goal of this thesis research is to explore if TC tornadoes can be successfully generated in real-case simulations without artificially inserting a tornado precursor, a method which is often used in idealized tornado simulations. The success of explicit simulation of TC tornado genesis and intensification in a real-case hindcasting mode opens a new avenue to tackle various issues of TC tornadoes that observations and idealized simulations cannot solely address. While none of our sensitivity experiments lead to changes in tornado behavior, we did

find that surface convergence was a consistent signal throughout our simulations that could have been falsely attributed to increased instability and reduced mid-level dry air. Future experiments will investigate the details of surface convergence on the dynamics of tornado formation.

LIST OF REFERENCES

Baker, A. K., Parker, M. D., & Eastin, M. D. (2009). Environmental Ingredients for Supercells and Tornadoes within Hurricane Ivan. *Weather Forecasting*, 223-244.

Carroll-Smith, D., Trapp, R. J., & Done, J. M. (2021). Exploring inland tropical cyclone rainfall and tornadoes under future climate conditions through a case study of Hurricane Ivan. Journal Of Applied Meteorology And Climatology, 60, 103-118. doi:10.1175/JAMC-D-20-0090.1

Curtis, L. (2004). Midlevel Dry Intrusions as a Factor in Tornado Outbreaks Associated with Landfalling Tropical Cyclones from the Atlantic and Gulf of Mexico. *Weather Forecasting*.

Deardorff, J. (1980). Stratocumulus-capped mixed layers derived from a three-dimensional model. *Boundary Layer Meteorology*.

Dudhia, J. (1989). Numerical Study of Convection Observed during the Winter Monsoon Experiment Using a Mesoscale Two-Dimensional Model. *Journal of the Atmospheric Sciences*.

Edwards, R. (2010). Tropical Cyclone Tornado Records for the Modernized National Weather Service Era. *25th Conference on Severe Local Storms*.

Edwards, R. (2012). Tropical Cyclone Tornadoes: A review of Knowledge in Research and Prediction. *Severe Storms Meteorology*.

Edwards, R., & Pietrycha, A. E. (2006). Archetypes For Surface Baroclinic Boundaries Influencing Tropical Cyclone Occurrence. *23rd Conf. on Severe Local Storms* (p. P8.2). St. Louis: American Meteorological Society.

Feliciano-Camacho, C. (2016). The impact of dry air on the location of tornado outbreaks associated with landfalling tropical cyclones in the Atlantic basin (thesis). .

Fiedler, B. H. (1994). The thermodynamic speed limit and its violation in axisymmetric numerical simulations of tornado-like vortices. *Atmosphere & Oceans*, 335-359.

Hill, E., Malkin, W., & Schulz, W. (1966). Tornadoes Associated with Cyclones of Tropical Origin-Practical Features. *Journal of Applied Meteorology and Climatology*.

Kain, J., & Fritsch, M. (1993). *COnvective Parameterization for Mesoscale MOdels: The Kain-Fritsch Scheme.*

Kolmogorov, A. (1941). The Local Structure of Turbulence in Incompressible Viscous Fluid for Very Large Reynolds' Numbers.

Lewellen, D. C., & Lewellen, W. S. (2000). The Influence of a Local Swirl Ratio on Tornado Intensification near the Surface. *Journal of Atmospheric Science*, 527-544.

Mashiko, W., Niino, H., & Kato, T. (2009). Numerical Simulation of Tornadogenesis in an Outer-Rainband Minisupercell of Typhoon Shanshan on 17 September 2006, Monthly Weather Review, 137(12), 4238-4260.

McCaul, E. W. (1991). Buoyancy and Shear Characteristics of Hurricane Tornado Environments. *Monthly Weather Review*, 119.

Mlawler, E., Taubman, S., & Brown, P. (1997). Radiative transfer for inhomogeneous atmospheres: RRTM, a validated correlated-k model for the longwave. *Journal of Geophysical Research*.

Molinari, J. (2008). Extreme helicity and intense convective towers in Hurricane Bonnie. *Monthly Weather Review*.

Molinari, J., & Vollaro, D. (2010). Distribution of Helicity, CAPE, and Shear in Tropical Cyclones. *Journal of the Atmospheric Sciences*, 274-284.

Novlan, D. J., & Gray, W. M. (1974). Hurricane-Spawned Tornadoes. *Monthly Weather Review*.

Onderlinde, M. J., & Fuelberg, H. E. (2014). A Parameter for Forecasting Tornadoes associated with Landfalling Tropical Cyclones. *Weather and Forecasting*, 1238-1255.

Orf, L. (2017). Evolution of a Long-Track Violent Tornado with a Simulated Supercell. *Bulletin of the American Meteorological Society*, 45-68.

Roberts, B., & Xue, M. (2016). The role of surface drag in tornadogenesis within an idealized supercell simulation. *Journal of the Atmospheric Sciences*, 3371-3395.

Schenkel, B. (2020). A Climatological Analysis of Ambient Deep-Tropospheric Vertical Wind Shear Impacts upon Tornadoes in Tropical Cyclones. *Weather Forecasting*.

Schneider, D., & Sharp, S. (2007). Radar Signatures of Tropical Cyclone Tornadoes in Central North Carolina. *Weather and Forecasting*, 278-286.

Schultz, L. A., & Cecil, J. D. (2009). Tropical Cyclone Tornadoes, 1950–2007. *Monthly Weather Review*.

Schubert, W. H., Montgomery, M. T., Taft, R. K., Guinn, T. A., Fulton, S. R., Kossin, J. P., & Edwards, J. P. (1999). Polygonal Eyewalls, Asymmetric Eye Contraction, and Potential Vorticity Mixing in Hurricanes, Journal of the Atmospheric Sciences, 56(9), 1197-1223.

Skamarock, W. C., & Klemp, J. (2008). A Description of the Advanced Research WRF Version 3.

Spartt, S. e. (1997). A WSR-88D assessment of Tropical Cyclone Outer Rainband Tornadoes. *Weather Forecasting*, 12, 479-501.

Sueki, K. (2016). Toward better assessment of tornado potential in typhoons: Significance of considering entrainment effects for CAPE.

Sukoriansky, S. (2005). Application of a new spectral theory of stably stratified turbulence to atmospheric boundary layers over sea ice. *Boundary Layer Meteorology*, 231-257.

Tewari, M. (2004). Implementation and Verification of the Unified Noah Land Surface Model in the WRF models. *20th Conference on Weather analysis*, 11-15.

Mashiko, W., Niino, H., & Kato, T. (2009). Numerical Simulation of Tornadogenesis in an Outer-Rainband Minisupercell of Typhoon Shanshan on 17 September 2006, Monthly Weather Review, 137(12), 4238-4260. Retrieved May 24, 2022, from https://journals.ametsoc.org/view/journals/mwre/137/12/2009mwr2959.1.xml

Xue, M. (2004). 4DVAR assimilation of ground temperature for the estimation of soil moisture and temperature. *Extended Abstracts, 20th Conference on Weather Analysis and Forecasting*.

Zhu, P. (2008). A Multiple Scale Modeling System for Coastal Hurricane Wind Damage Mitigation. *Natural Hazards*.

Zhu, P. (2008). simulation and Parameterization of the Turbulent Transport in the Hurricane Boundary Layer by Large Eddies. *Journal of Geophysical Research*.

Zhu, P. e. (2015). The sensitivity of simulated shallow cumulus convection and cold pools to microphysics. *Journal of Atmospheric Science*.